

LATITUDE-DEPENDENT EFFECTS IN THE STELLAR WIND OF ETA CARINAE¹

Nathan Smith² and Kris Davidson

Astronomy Department, University of Minnesota, 116 Church St. SE, Minneapolis, MN 55455

Theodore R. Gull

Laboratory for Astronomy and Space Science, NASA/Goddard Space Flight Center, Greenbelt, MD 20771

Kazunori Ishibashi

Center for Space Research, Massachusetts Institute of Technology, 77 Massachusetts Ave., Cambridge, MA 02139

D. John Hillier

Department of Physics and Astronomy, University of Pittsburgh, 3941 O'Hara Street, Pittsburgh, PA 15260

ABSTRACT

The Homunculus reflection nebula around η Carinae provides a rare opportunity to observe the spectrum of a star from more than one direction. In the case of η Car, the nebula's geometry is known well enough to infer how line profiles vary with latitude. We present STIS spectra of several positions in the Homunculus, showing directly that η Car has an aspherical stellar wind. P Cygni absorption in Balmer lines depends on latitude, with relatively high velocities and strong absorption near the polar axis. Stronger absorption at high latitudes is surprising, and it suggests *higher mass flux toward the poles*, perhaps resulting from radiative driving with equatorial gravity darkening on a rotating star. Reflected profiles of He I lines are more puzzling, offering clues to the wind geometry and ionization structure. During η Car's high-excitation state in March 2000, the wind was fast and dense at the poles, with higher ionization at low latitudes.

Older STIS data obtained since 1998 reveal that this global stellar-wind geometry changes during η Car's 5.5 year cycle, and may suggest that this star's *spectroscopic events are shell ejections*. Whether or not a companion star triggers these outbursts remains ambiguous. The most dramatic changes in the wind occur at low latitudes, while the dense polar wind remains relatively undisturbed during an event. The apparent stability of the polar wind also supports the inferred bipolar geometry. The wind geometry and its variability have critical implications for understanding the 5.5 year cycle and long-term variability, but do not provide a clear alternative to the binary hypothesis for generating η Car's X-rays.

Subject headings: circumstellar matter — stars: individual (η Carinae) — stars: mass loss — stars: winds, outflows

¹Based on observations made with the NASA/ESA *Hubble Space Telescope*, obtained at the Space Telescope Science Institute, which is operated by the Association of Universities for Research in Astronomy, Inc., under NASA contract NAS5-26555.

²Current address: Center for Astrophysics and Space Astronomy, University of Colorado, 389 UCB, Boulder, CO 80309; nathans@casa.colorado.edu

1. INTRODUCTION

At visual wavelengths, the dusty bipolar “Homunculus” ejecta structure around η Car is primarily a hollow reflection nebula (see Thackeray 1961; Visvanathan 1967; Meaburn 1987; Hillier & Allen 1992; Hamann et al. 1994; etc.). Therefore, by observing localized parts of the Homunculus, *we can indirectly see the star’s spectrum from a range of directions in space* — potentially allowing us to reconstruct the shape of η Car’s wind, which is expected to lack spherical symmetry. Independent of the large-scale bipolar morphology, hints of non-sphericity have been noted by, e.g., Viotti et al. (1989), Hillier & Allen (1992), Davidson et al. (1995), Davidson & Humphreys (1997), and Zethson et al. (1999). Indeed, Hillier & Allen (1992) found a difference between direct and reflected He I emission that originates in the stellar wind, and early Space Telescope Imaging Spectrograph (*HST*/STIS) observations showed that the reflected H α profile depends on location within the Homunculus.

Departures from spherical symmetry are obviously critical for theories of winds and instabilities in the most massive stars (see Lamers & Cassinelli 1999, and papers in Wolf, Stahl, & Fullerton 1998). Asphericity in η Car’s wind may also be critical for understanding its 5.5 year cycle (Damineli 1996), its long term variability, and excitation of its ejecta. In addition to its classic status as a very massive unstable star, η Car is uniquely favorable for this problem because the dusty Homunculus has a fairly definite three-dimensional structure; each projected location on the nebula provides reflected light from a viewing direction whose stellar latitude is approximately known (Davidson et al. 2001; Smith 2002).

We have obtained long-slit STIS spectra optimized for studies of the reflected latitude-dependent effects. We find that some features do in fact depend on viewing direction. Wind velocities are highest around the pole, as one might expect if stellar rotation reduces the effective gravity and escape velocity at the equator. Dominant outflow velocities in the stellar wind are 400 to 600 km s $^{-1}$, but some faster material (\sim 1000 km s $^{-1}$) had been seen (Viotti et al. 1989; Damineli et al. 1998), and our data now show that these high velocities are polar. We also find a much less anticipated phenomenon: broad P Cyg absorption components of H α and H β , usually weak in our direct view of η Car, *are quite deep at higher (not lower) latitudes*. Traditionally, a slow equatorial wind is supposed to be denser than the associated fast polar wind and the mass-loss rate may increase with decreasing g_{eff} (Friend & Abbott 1986); some examples are B[e] stars (Zickgraf et al. 1986), wind-compressed disks or zones (Bjorkman & Cassinelli 1993; Ignace, Cassinelli, & Bjorkman 1996; Owocki, Cranmer, & Blondin 1994), and bistable winds (Lamers & Pauldrach 1991). Our observations of η Car, however, suggest that its wind is densest near the poles despite higher velocities there. Other interpretations are conceivable, but require detailed models of line transfer.

If η Car’s wind densities are highest near the poles as one might guess from the deeper hydrogen P Cyg absorption, then this tends to support recent comments by Owocki and others concerning the importance of non-radial forces and gravity darkening in line-driven winds of massive stars (Owocki, Cranmer, & Gayley 1996; Owocki & Gayley 1997; Owocki, Gayley, & Cranmer 1998; Maeder & Meynet 2000; Meader & Desjacques 2001). Specifically, these studies predict that if a luminous star is rotating fast enough for gravity darkening to be important (i.e., at \gtrsim 70% of the “critical” rotation speed), then stronger radiative flux at the hot poles will tend to drive a higher mass flux. Glatzel (1998) and Maeder (1999) have discussed modifications to the “critical” rotation rate near the Eddington luminosity.

We describe new STIS observations in §2 below, hydrogen line profiles in §3, and helium profiles in §4. In §5 we discuss various likely implications of the observed wind geometry. Then in §6 we examine older STIS spectra and discuss temporal variability of the wind structure. Finally, in §7 we mention consequences that a variable, bipolar wind may have for interpretations of η Car’s 5.5-year spectroscopic cycle.

2. STIS SPECTRA OF THE HOMUNCULUS

These observations are part of an intensive *HST*/STIS project to study η Car and the Homunculus during their current 5.5-year spectroscopic cycle (Davidson et al. 1999, 2000, 2001; Gull et al. 1999; Gull & Ishibashi 2001). Early observations in March 1998 and February 1999 used only a narrow $0.1''$ -wide STIS slit with short exposures, inadequate for outer parts of the Homunculus (although we did obtain a few deeper exposures at wavelengths near $H\alpha$ that were offset from the star; see below). Moreover, difficulties in scheduling *HST* prevented the slit from being aligned closely with the Homunculus bipolar axis during those earlier observations. Therefore, we planned a special set of STIS observations with a wider $52'' \times 0.2''$ aperture and longer exposures, and with a slit orientation closer to the Homunculus axis at position angle $138^\circ.9 \leftrightarrow 318^\circ.9$, as shown in Figure 1. Here we discuss observations sampled with STIS gratings G430M and G750M at standard tilts that gave central wavelengths of 4961, 6768, and 7283 Å. Achieved on 2000 March 13, these are the same data used in a paper on the Homunculus shape (Davidson et al. 2001). In order to reduce scattered light we occulted the star with a $0.65''$ bar across the slit, but other STIS observations gave a direct view of the star a week later (see below). Figure 2 shows examples of long-slit STIS spectra for a few bright reflected emission lines in η Car’s stellar wind (reflected continuum has been subtracted).

To study positional variation of line profiles in the Homunculus, we made several spectral extractions at positions along the slit listed in Table 1. Positive offsets are NW of the star, and negative offsets are SE.³ The spectrum at each offset position has a net redshift, due to reflection by expanding dust. We corrected for this effect by aligning the blue side of the $H\alpha$ emission line profile at 10 times the continuum flux (however, a different choice would not alter the results substantially because the profiles match well). The net shift applied at each position is given as Δv in Table 1. We used these values of Δv to correct the apparent velocities of other emission lines discussed later. Each resulting line profile samples the spectrum of the central star seen from different positions in the reflection nebula, and each corresponds to a different latitude as depicted in Figure 3. This technique works because the polar lobes are mostly hollow, as indicated by limb-brightening in thermal-infrared images (e.g., Smith et al. 1998, 2002).

The case of η Car is unique, because the geometry of the bright, hollow reflection nebula is known sufficiently well that we can correlate position in the nebula with stellar latitude (assuming that the polar axis of the star and nebula are aligned – in this case the assumption is justified by the results, see §3). Davidson et al. (2001) estimated the shape and orientation of the Homunculus from the same dataset used here, and we use their “compromise” shape (shown in Figure 3) to derive the latitude for each extraction position as listed in Table 1 and depicted in Figure 3. Since the Homunculus may not be fully axisymmetric, our estimated latitudes have uncertainties of roughly $\pm 5^\circ$. The axis for the southeast Homunculus lobe is tilted at $i \approx 41^\circ \pm 2^\circ$ relative to our line of sight (see Davidson et al. 2001; Smith 2002).

The 2000 March 13 observations used a $0''.65$ bar to occult the central star, but other STIS spectra obtained on 2000 March 20 sampled the star with a $0''.1$ -wide slit. A $0''.15$ segment was extracted from the 2000 March 20 data for all emission lines discussed here. We also examined the spectrum of one position in the equatorial ejecta located $\sim 5''$ NE of the star, constructed from several adjacent slit positions used to map the Homunculus at wavelengths near $H\alpha$ on 2000 March 21. The extracted spectrum covers an effective area of $1'' \times 1''$, represented by the box labeled “NE 5” in Figure 1. This spectrum is discussed in §5.4 (and see Table 1). Temporal variations should not introduce significant errors since the datasets were taken only

³Table 1 lists information for $H\alpha$ profiles, but the same extractions were made for other emission lines discussed later. Some offsets listed in figures for other emission lines differ from those in Table 1, because adjacent tracings were combined to increase signal-to-noise.

1 week apart, while differences in light travel times for reflected light from the SE polar lobe are only a few weeks or less. Thus, the observed variation in line profiles *along the slit* cannot be due merely to temporal variations in the spectrum.

In §6 we investigate temporal variability of reflected profiles as seen in STIS spectra obtained with the G750M grating (central wavelength = 6768 Å) on 1998 March 19 and 1999 February 21. These are long-slit spectra similar to those obtained on 2000 March 13, but were obtained using a 0''.1-wide slit located 0''.4 NW of the star at position angle 152°1↔332°1, as shown by the dotted line in Figure 1. Transformation between position along the slit and corresponding stellar latitude is less straightforward than for the March 2000 data. For the 1998 and 1999 data, we estimated latitudes for each offset position using contours superimposed on images of the Homunculus (Davidson et al. 2001). Uncertainty in latitude for these extractions is about $\pm 5^\circ$. Spectra of the star for comparison with reflected spectra were obtained simultaneously, and processed in the same manner as stellar spectra discussed above. In context with variability during η Car's 5.5 year spectroscopic cycle (Damineli 1996), STIS observations in March 1998, February 1999, and March 2000 occur at phases of 0.04, 0.21, and 0.4, respectively (see §5.1.2 and §7).

In §3 we discuss a small portion of the ultraviolet STIS FUV/MAMA spectrum of η Carinae, obtained in echelle mode with the E140M grating on 2000 March 23, using a 0''.2 × 0''.2 aperture centered on the central star. These data are used here to help understand aspects of the optical spectra; a detailed analysis of the UV spectra will be presented in a future publication.

3. HYDROGEN LINE PROFILES

3.1. Latitudinal Dependence of P Cygni Absorption

Figure 2 shows that reflected line profiles vary with position along the slit. The primary change occurs in strength and velocity range of hydrogen P Cygni absorption, which is strongest 5'' to 6'' SE of the star. P Cygni absorption is weak in the directly-observed star and in reflected light from the NW lobe. H β and H α profiles agree well (Figures 4 and 5); their scattering wings and emission peaks vary little across the SE lobe, but absorption components depend on position. Absorption traces a more direct and narrow line of sight between reflecting dust in the polar lobes and the star (this is particularly true for Balmer absorption, which occurs at large radii compared to the continuum), whereas emission comes from a range of latitudes.⁴ Since each position along the slit translates to a line of sight down onto a different latitude on the central star, P Cygni absorption components give direct evidence that the density and/or ionization structure of η Car's current stellar wind is non-spherical. The possible cause of this aspherical structure is addressed in §5.

To quantify the latitudinal dependence of velocity, we measured “terminal” speed v_∞ and minimum-flux speed v_{pcyg} for each tracing in Figure 4. Figure 6 shows how we defined these two velocities observationally, and resulting measurements are listed in Table 1. With data from Table 1, Figure 7 indicates how observed expansion velocities vary with latitude. Changes in v_∞ are greater than the uncertainty, which could be up to 100 km s $^{-1}$ for high latitudes. For our line of sight, v_∞ measured in Balmer lines is within ~ 50 km s $^{-1}$ of the terminal velocity indicated by UV wind lines, like Si II $\lambda 1527$, also observed in March 2000 using the STIS FUV/MAMA detector (Figure 8). Several aspects of hydrogen emission-line profiles in Figures 4 and

⁴It is unlikely that the very broad P Cygni absorption features arise in material within the polar lobes or outside them, because intrinsic emission lines at those locations have narrow line widths (see Davidson et al. 2001; Hillier & Allen 1992).

5, and trends in Figure 7 deserve comment:

1. *Higher velocities near the pole.* Blueshifted absorption is seen at speeds up to $\sim 1100 \text{ km s}^{-1}$, which is much faster than values usually quoted for η Car’s stellar wind. The fastest material between 5'' and 6'' SE of the star nearly coincides with the polar axis of the Homunculus. In Figure 7, the measured quantities v_∞ and v_{pcyg} both follow a similar trend of smoothly increasing speed with latitude, and there appears to be a rather extreme increase in v_∞ close to the polar axis.

2. *Deeper absorption near the pole.* Perhaps the most significant and surprising result of this investigation is that the deepest P Cygni absorption in Balmer lines is seen at the polar axis, with absorption weakening *progressively* toward lower latitudes (see Figure 5). At latitudes below about 40° , the normal Balmer P Cygni absorption is absent in the wind⁵. In dense winds like η Car’s, the strength of P Cygni absorption in Balmer lines is sensitive. It depends on the population of the $n = 2$ state and is not necessarily a direct tracer of column density. Weak Balmer absorption at low to mid latitudes could be due to higher ionization in that part of η Car’s wind, lower density, or a subtle combination of both effects.

3. *Symmetry about the equatorial plane and polar axis.* Measured values of v_∞ and v_{pcyg} plotted together in Figure 7 follow the same trend regardless of which polar lobe or which side of the SE polar axis they correspond to. Also, H α emission and absorption profiles on either side of the pole are identical. This indicates that the wind outflow pattern is *axisymmetric*.

3.2. Enhanced Emission from the Star

Electron scattering wings and line peaks seen at various positions in the SE polar lobe all have the same profile shape (excluding blueshifted absorption), but these reflected profiles all differ from our direct view of the central star. The difference is considerable – almost a factor of 2 in the peak intensity (Figure 5 has a logarithmic scale). Our direct view of the central star shows stronger emission at velocities between about -250 and $+500 \text{ km s}^{-1}$ in both H β and H α , but broad scattering wings are consistent with profiles seen in reflection. Apparently, when we look at the star we see extra line emission (or extra continuum opacity) that is not seen by reflected lines of sight; the opposite case would have been easier to explain. A similar but lesser effect appeared in the *HST/FOS* data on H β (Davidson et al. 1995; see also Hillier et al. 2001). Later (in §6 and Figure 16) we show that this characteristic of the star’s emission persists at roughly the same level throughout η Car’s spectroscopic variability cycle.

Models of the central star’s spectrum (as seen in March 1998) by Hillier et al. (2001) showed a related problem: The model adequately reproduced the electron scattering wings, but underestimated peak emission of Balmer lines. The model also overestimated the strength of P Cygni absorption. Thus, the atmosphere model used by Hillier et al. approximates the reflected spectrum from the polar lobes in March 2000 more closely than it does the central star’s spectrum, although the observed outflow velocities at high latitudes exceed the 500 km s^{-1} terminal velocity adopted in their model. This problem may be related to wind geometry, since Hillier et al. assumed spherical symmetry.

Fe II Profiles. Figures 9 and 10 show observed emission-line profiles for Fe II $\lambda 4925$, extracted from positions across the Homunculus and the central star in the same manner as Balmer line profiles shown in

⁵This transitional latitude in the wind properties may have broader implications, since it corresponds to the approximate division between the caps and walls of the bipolar lobes (see Davidson et al. 2001; Smith 2002).

Figures 4 and 5. Fe II $\lambda 4925$ is a bright permitted line in η Car's wind, and shows a broad profile similar to many other Fe II lines.⁶ Fe II and H α emission show a similar latitudinal dependence. Namely, the velocity and to some extent the strength of P Cygni absorption increase with latitude. Also, Fe II emission from the central star is stronger than at reflected positions. Thus, a solution to this problem for Balmer line emission should also account for the Fe II discrepancy. More importantly, the similar behavior of these two lines suggests that they arise in the same outer zone of η Car's wind, as expected because the ionization of Fe II is coupled to H by charge exchange in dense stellar winds.

4. HELIUM LINE PROFILES

Figure 2 shows the long-slit spectrum across the major axis of the Homunculus for He I $\lambda 7067$ and $\lambda 6680$. Tracings for both He I $\lambda 6680$ and $\lambda 7067$ at several reflected positions across the nebula and for the central star are shown in Figures 9 and 10. Reflected line profiles in the SE lobe seem to have three velocity components in Figure 2, caused by a combination of a narrow central component from circumstellar gas, plus a broad plateau or double-peaked line arising in the wind.

Contamination by reflected narrow He I $\lambda 7067$ emission from circumstellar ejecta like the Weigelt blobs (see Davidson et al. 1995, 1997) needs to be examined before the wind lines can be interpreted. At 2" to 4" SE of the star, narrow emission is conspicuous but the broad component and the continuum emission fade. This suggests that obscuring dust lies along this particular line of sight to the star, projecting a *shadow* onto the SE polar lobe. This same position corresponds to a relatively dark region in color *HST* images of the Homunculus (see Figure 1 and Morse et al. 1998). Intervening material must be close to the star (within ~ 3500 AU) and compact ($r \lesssim 200$ AU), because it obscures the star along this line of sight but does not block the Weigelt blobs. The dust in question may be in condensations analogous to the Weigelt blobs themselves. Dense dust knots seen at thermal-infrared wavelengths (Smith et al. 2002) are good candidates for such blobs that are casting shadows. Perhaps some other dark spots in the Homunculus are also shadows cast by inner debris, rather than holes or dense patches.

Changes in broad stellar-wind profiles are complicated, and may be affected by a hypothetical companion star. However, some clues to the overall wind structure can be gathered. Broad He I $\lambda 7067$ emission in the SE lobe (see Figure 9) has a nearly symmetric profile. This broad profile, combined with the central narrow component, creates the triple-peaked appearance of He I $\lambda 7067$ in the SE lobe in Figure 2. The red side of He I lines disappears in the reflected spectra from the NW polar lobe, in the spectrum of the star, and in reflected spectra in the SE polar lobe at positions near the star (see Figures 9 and 10). The blue side of the broad He I line profiles is much stronger in the NW lobe, but roughly the same for the SE lobe and central star (Figure 10). In other words, low latitudes (below $\sim 50^\circ$) seen from the NW lobe have asymmetric profiles with extra blueshifted emission, whereas high latitudes in the SE lobe show symmetric profiles and extra redshifted emission compared to the central star. It is more difficult to ascertain the level of axisymmetry in He I emission than for Balmer lines, because He I lines do not show such drastic changes near the pole; He I emission does appear to be symmetric about the equatorial plane.

The central star and reflected emission from the NW lobe (low latitudes) also show P Cygni absorption at -400 km s $^{-1}$ in He I lines, but the reflected spectra in the SE lobe (high latitudes) do not. Balmer lines

⁶Fe II $\lambda 4925$ is blended with He I $\lambda 4923$, but the observed latitudinal behavior of this line profile in comparison with other Fe II and He I lines suggests that it is dominated by the Fe II transition.

show the opposite trend; namely, stronger P Cygni absorption at high latitudes. Important He I lines at 10830 and 20581 Å also show P Cygni absorption (Hamann et al. 1994; Damineli et al. 1998; Smith 2001, 2002); it would be interesting to see how these vary with latitude. Continued monitoring of direct and reflected He I line profiles during η Car’s 5.5 year cycle with STIS may provide a powerful diagnostic of the stellar wind’s complex ionization structure.

5. WIND STRUCTURE DURING THE NORMAL HIGH-EXCITATION STATE

Latitudinal variations of H and He I lines described above show that the speed, density, and ionization in η Car’s wind are non-spherical. Do these indicate an inherently axisymmetric wind, or is the structure influenced by a hypothetical hot companion star? One can imagine suitable parameters for a binary model, but in several ways described below the observations more closely match theoretical predictions for a dense line-driven wind from a rotating star (Owocki et al. 1996, 1998; Owocki 2002). Thus, we favor rotation of the primary star as the dominant factor shaping η Car’s wind.

5.1. A Non-spherical Stellar Wind?

5.1.1. Latitudinal velocity dependence

Figure 7 shows maximum outflow velocities increasing rapidly toward the poles. If the terminal speed v_∞ is proportional to the escape speed as usually occurs in stellar-wind theory, and if the surface rotation rate Ω does not perceptibly depend on stellar latitude β , then one might expect a simple latitude dependence:

$$v_\infty(\beta) \approx v_\infty(\text{pole})\sqrt{1 - q^2\cos^2\beta} \quad (1)$$

where $q \approx v_{\text{rot}}/v_{\text{crit}}$ and $v_{\text{crit}} \equiv \sqrt{GM/R}$ at the equator. Higher polar velocities are generally expected from any rotating star with lower effective gravity at the equator. An example of this trend is shown in Figure 7 for $q = 0.9$, and obviously does not match the observed latitude dependence exactly. But this failure is not very surprising since the assumption ignores possible complications; line-driven wind theory may be an oversimplification for η Car, opacity may depend on latitude, the flow is not necessarily radial, etc. However, the ratio of the polar to equatorial velocities does seem marginally consistent with $q = 0.9$.

The rapid rise in v_∞ toward the pole is somewhat problematic, especially since no high-speed redshifted emission is seen there. Fast material may be concentrated in a narrow cone near the polar axis, so it may not contribute significantly to the H α -emitting volume in the wind. This must be addressed with quantitative modeling. A normal binary model offers no obvious explanation for high polar wind velocities, especially since one expects the orbital plane to be roughly aligned with the equator of the star and Homunculus. High velocities seen in reflected light from the SE polar lobe give the first direct indication that the polar axis of the Homunculus is aligned with the rotation axis of the central star. The alignment of these axes has important consequences for the formation of the bipolar lobes and equatorial ejecta around η Car. Namely, it means that axial symmetry and ejection physics during the Great Eruption may be directly linked to the star’s rotation (see §5.5).

High velocities seen in reflection also indicate fast-moving material somewhere inside the Homunculus, but the absorption probably occurs relatively close to the star and not in the middle of the polar lobes or

outside them (see §6.3). Values for v_∞ at high latitudes are almost twice the expansion velocities for gas and dust in the Homunculus (see Figure 7). Therefore, we should expect shock-excited emission inside the polar lobes as the stellar wind overtakes slower material from the Great Eruption (Smith 2001, 2002; Smith & Davidson 2001).⁷ The highest speeds we observe in η Car’s wind and Homunculus are insufficient for η Car’s hard X-rays, which presumably require shock velocities of roughly 3000 km s^{-1} (Corcoran et al. 1995; Ishibashi et al. 1999; Pittard & Corcoran 2002).

5.1.2. *Colliding winds and axisymmetry*

The weakness or absence of P Cygni absorption in Balmer lines at low latitudes and the strange latitudinal behavior of He I lines make a colliding-wind binary model worth considering. A hot companion star’s wind might sculpt part of the dense primary wind (see, e.g., Pittard & Corcoran 2002) and ionize its equatorial zones, but a binary model does not give an obvious explanation for the fast polar wind. If high speeds are induced by a companion star, we might expect them primarily at low latitudes instead.

However, one argument against a companion star dominating the wind structure is that the non-spherical wind appears to be *axisymmetric*, as noted in §3.1. In Figure 7, velocities from both hemispheres and both sides of the polar axis follow the same smooth latitudinal dependence, and P Cygni absorption in hydrogen lines has the same depth on either side of the pole. The evidence for axisymmetry is not as clear in He I emission profiles, but they are consistent with an axisymmetric wind. If η Carinae has a companion star that causes colliding-wind X-ray emission, it must have a very eccentric orbit (see contribution in Morse et al. 1999). The STIS observations described here were obtained in March 2000, when a companion would be nearly at apastron. The shock would be between the two winds, while the far side of the primary star’s wind should be mostly unaffected – a seriously asymmetric arrangement.

Therefore the basic stellar-wind geometry most likely results from the star’s rotation. A hypothetical hot companion may help to explain the He I emission and other effects, but this has not been demonstrated and requires theoretical work.

5.2. **Density or Ionization?**

To understand the wind structure, we first need to recall how density and ionization govern the behavior of P Cygni absorption in H α and H β . Balmer absorption in dense stellar winds is sensitive to changes in wind ionization structure, but that ionization structure in turn depends sensitively on density. Najarro, Hillier, & Stahl (1997) present a detailed analysis of the behavior of H and He I lines in the spectrum of P Cygni. Much of their analysis may be applicable to η Car’s wind (see also Hillier et al. 2001). They find that in dense winds of hot stars, the appearance of Balmer lines falls into one of two regimes, depending on H recombination. Dense winds that remain fully ionized show pure H emission profiles. If hydrogen recombines, however, the population of the $n=1$ state increases dramatically, and so the Lyman series and Lyman continuum become optically thick. Because of high optical depth in Ly α , the $n=2$ state acts as a metastable level and gives rise to strong Balmer absorption. Essentially, Najarro et al. find that strong Balmer absorption requires sufficient density to cause H recombination in the outer wind. This is evidently

⁷In addition, there appears to be some evidence for weak non-thermal radio emission from the edges of the Homunculus (White 2002).

the case for η Car’s polar wind; much weaker Balmer absorption toward low latitudes then suggests that H remains mostly ionized there. Najarro et al.’s calculations show that even a small reduction in the mass-loss rate can prevent H recombination; Hillier et al. (2001) comment that for η Car, dramatic changes in P Cygni absorption are seen if the mass-loss rate in their model is lowered by factors of 2 to 4. Thus, we can explain increasing strength of Balmer absorption toward the pole if η Car’s wind has a *latitudinal density gradient, with higher densities toward the pole*. Evidently, the wind begins to reach a critical level for recombination near latitudes of 40° . This is analogous to (but opposite) the “bistability” model for B[e] supergiants (Lamers & Pauldrach 1991; Pauldrach & Puls 1990).

Figure 11 shows a hypothetical picture of latitudinal structure in η Car’s stellar wind during its normal high-excitation state. The inner circle represents the stellar radius, which is somewhat ambiguous because the wind is opaque (see Hillier et al. 2001, Davidson et al. 1995). Figure 11 depicts two different zones in η Car’s outer wind: 1) a high-density, low-ionization zone where H recombines and produces Balmer absorption (shaded), and 2) a lower density, high-ionization zone (hatched) producing the He I emission, or at least relatively transparent so that more of the underlying He I zone is seen, and where H remains ionized. In reality, of course, demarcation between these zones is not so sharp. More theoretical work is needed to understand the observed line profiles (especially He I), but this picture qualitatively satisfies the main observational requirements of preceding sections:

Polar View: Seen from the pole, the spectrum shows deep, high-velocity P Cygni absorption in Balmer and Fe II lines through dense regions of the recombined wind. Looking through relatively transparent extended He I emission zones on either side of the star, an observer sees a symmetric He I profile, with blue- and red-shifted velocities of similar intensity out to about $\pm 400 \text{ km s}^{-1}$. P Cyg absorption is weak or absent in He I lines toward the poles, since there is no continuum source behind these extended He I-emitting zones.

Low Latitudes: The low density and high-ionization at low latitudes inhibit hydrogen P Cyg absorption in Balmer lines and favor He I emission. An observer will see stronger blueshifted He I lines from deeper in the wind than other latitudes, since redshifted He I emission is occulted by the star.

Intermediate Latitudes (Our Line of Sight): We see weaker hydrogen P Cygni absorption than a polar observer because we see more continuum from deeper in the hotter parts of the wind; for a polar observer, all the continuum and electron scattering is behind the absorbing region of the wind. We also see mostly blueshifted He I emission, but not as strong as for viewpoints at lower latitudes because the He I is spread over a wider velocity range, and because our line-of-sight is nearly along the transition between the two zones. The recombined polar region of the wind does not emit as much He I and is responsible for the missing (or weaker) blueshifted peak in the star’s He I line profile as compared to the NW lobe.

5.3. Rotational Wind Compression

The above results suggest that η Car’s wind has prolate mass flux, with higher velocities, higher densities, and lower ionization toward the pole. This is surprising, because reduced effective gravity at the equator of a rotating star might lead one to expect the opposite; for example, rapidly rotating B[e] supergiants are thought to have low-ionization equatorial density enhancements, as noted earlier. However, the prolate mass flux we observe in η Car during its normal high-excitation state is not without theoretical precedent.

Considering only centrifugal forces in an expanding and rotating wind, one might expect material to be deflected toward the equator (e.g., Bjorkmann & Cassinelli 1993). However, in a line driven wind

other factors are important; radiation-hydrodynamical simulations that include non-radial forces with CAK (Castor, Abbott, & Klein 1975) formalism for line-driven winds show that equatorial density enhancements can be inhibited (Owocki et al. 1996, 1998). Furthermore, with gravity darkening, oblateness, and other effects, Owocki et al. predict enhanced mass flux toward the polar directions of a rotating star. Analytic scaling laws from CAK theory (their equation 46) can be modified to give an approximate relation (see Owocki et al. 1996) for the dependence of local mass-loss rate on flux F and gravity g_{eff} , given by

$$\dot{M} \propto F^{\frac{1}{\alpha}} g_{eff}^{1-\frac{1}{\alpha}} \quad (2)$$

where α is the force multiplier power-law index that is usually adopted in CAK theory. However, the prologue to von Zeipel's theorem predicts that $F \propto g_{eff}$ for a rotating star.⁸ If this relation applies, if rotation is responsible for η Car's asymmetry, and if line-driven wind theory is a fair approximation, then equation (2) implies that local mass flux ρv should be proportional to g_{eff} , which depends on latitude. Since v tends to be more or less proportional to $\sqrt{g_{eff}}$, we expect, very crudely, a wind density dependence $\rho \propto \sqrt{g_{eff}}$. Thus, the polar wind density can easily be higher than that near the equator. Figure 7 suggests that the ratio might be as large as 2, which, as noted in §5.2, may allow deep P Cygni absorption features at the pole but not at low latitudes. Even if the above argument does not strictly apply, some modifications to the theory for luminous stars tend to produce strong polar mass flux (see, e.g., Maeder 1999; Maeder & Desjaques 2001). Here we have ignored obvious possibilities of latitudinal opacity variations and of acceleration by the radiation continuum; a quantitative investigation is merited but will be difficult.

The essential requirement of our proposed interpretation of η Car's wind asymmetry – that higher densities toward the pole lead to recombination at large distances in the wind (as discussed by Najarro et al. 1997) – seems theoretically plausible if η Car is rotating rapidly enough to cause equatorial gravity darkening (see Owocki et al. 1996, 1998; Owocki & Gayley 1997).⁹ Gravity darkening on the star would not necessarily contradict the higher ionization observed at low/mid latitudes in the wind, because that latitude-dependent ionization is regulated by the local density instead of an anisotropic UV source (§5.2). For instance, latitudes at $\sim 25^\circ$ from the equator should still “see” the hot pole of the star. Material much closer to the equator will have a more difficult time getting UV radiation from the hot poles, leading one to expect lower ionization there; this may indeed be the case, as discussed in the next section.

While higher polar velocities are a generic property of winds from rotating stars, higher polar mass flux is a distinctive property of line-driven winds with gravity darkening. Thus, our observations appear to support the hypothesis that η Car's present-day stellar wind is in fact radiatively driven. This may not hold true during the Great Eruption.

⁸Some authors call the above relation “von Zeipel's theorem”, but in fact it is merely a preliminary to the theorem itself, which dealt with a more complex problem. See Eddington (1926), Kippenhahn & Weigert (1990), and von Zeipel (1924).

⁹One should bear in mind, however, that the observed H α and H β absorption features represent the NLTE population of the $n = 2$ level, which depends on various subtle factors. Some of these, such as three-dimensional velocity gradients, are not treated adequately in any published wind models.

5.4. An Equatorial Disk?

Several authors have discussed evidence for strange kinematics in η Car’s equatorial ejecta (Zethson et al. 1999; Smith & Gehrz 1998; Morse et al. 2001; Davidson et al. 2001; Davidson & Humphreys 1997). Not all equatorial structures are coeval with the polar lobes ejected during the Great Eruption. The Homunculus’ ragged *equatorial* structure distinguishes it from other bipolar nebulae. Equatorial outflow in the present-day wind may be important for understanding this larger-scale morphology.

Figure 4 includes the equatorial H α profile observed $\sim 5''$ NE of the central star¹⁰ (see Figure 1), and Table 1 lists values of v_∞ and v_{pcyg} for this feature. These outflow velocities are higher than the expected trend at the equator, and deep P Cyg absorption there contradicts the observation that blueshifted absorption weakens with decreasing latitude. Thus, the reflected spectrum from NE 5 suggests that these trends reverse at the equator — perhaps indicating the presence of a dense equatorial disk. NE 5 might be peculiar since it is projected along a line from the star to the NN “jet” (see Morse et al. 1998; Meaburn et al. 1993). However, other STIS data obtained in November 1998 (not shown), with the slit crossing other extended parts of the equatorial skirt, also show obvious P Cygni absorption at the equator. Binary models that invoke a strong wind from a companion star (e.g., Pittard & Corcoran 2002) would seem to impede the survival of such a thin equatorial disk.

Perhaps some material escaping from mid-latitudes on the star is deflected toward the equator — in which case the same process may cause both depletion of the outer wind density at mid-latitudes and increased density near the equatorial plane. Various theoretical ideas including centrifugal wind compression and magnetic fields may produce an outflowing equatorial disk in this way (Bjorkman & Cassinelli 1993; Washimi & Shibata 1993; Balick & Matt 2001; ud-Doula & Owocki 2002; Lee, Saio, & Osaki 1991). Alternatively, low ionization in the “disk” may be related to the star’s gravity darkening (§5.3).

5.5. Shape and Structure of the Homunculus

The bipolar geometry depicted in Figure 11 naturally leads one to wonder if the present-day stellar wind’s bipolarity on small scales (within ~ 100 AU) is related to the shape and structure of the Homunculus Nebula on much larger scales. Conditions in η Car’s wind during the Great Eruption were very different than today, but let’s assume for the moment that the geometry of the mass loss was similar then.

Suppose that latitudinal dependence on density in η Car’s wind 160 years ago resembled Figure 11, but that during the eruption the mass-loss rate increased by a factor of 100 for 20 years — turned on and off like a faucet. In that case, most mass would have been ejected toward the poles during that time, forming two thick polar caps. Their radial thickness would be roughly $v \times 20 \text{ yr} \approx 2500 \text{ AU} \approx 1''$. This simple estimate matches observations; the Homunculus polar caps are indeed roughly 1'' thick at radii around 8'' from the star (Smith et al. 1998, 2002; Davidson et al. 2001).

This outburst scenario differs from previous hydrodynamic models for the formation of the Homunculus that invoke wind interactions to explain the observed bipolarity (e.g., Frank et al. 1995, 1998; Dwarkadas

¹⁰This location unambiguously represents equatorial ejecta, since it is not projected against the NW Homunculus lobe in images (see Figure 1). Some other apparently equatorial features superimposed on the lobe may be illusory. For instance, the “fan” a few arcsec northwest of the star is really a hole in the equatorial extinction, allowing that part of the NW lobe to appear brighter (Smith et al. 1999, 2002). Note that the STIS spectrum at NE5 does not include the entire 1'' box (see Table 1).

& Balick 1998; Langer et al. 1999). We should not expect post-eruption hydrodynamic effects to dominate the structure of the Homunculus, since material ejected during the eruption was a factor of 100 more dense but had comparable velocities to the pre- and post-eruption winds. Ram pressure in the post-eruption wind is insufficient to dominate the shape of the nebula or cause significant acceleration. Proper motions of the Homunculus ejecta (Morse et al. 2001; Smith & Gehrz 1998; Currie et al. 1996) indicate linear expansion. A bipolar eruption of a rotating star seems the best explanation for the basic Homunculus morphology (see Owocki & Gayley 1997; Maeder & Desjacques 2001; Dwarkadas & Owocki 2002).

Small-scale structure in the Homunculus lobes may also be related to details in the eruptive wind. Davidson et al. (2001) noted that the smallest observed feature size, about $0.1''$ (see Figure 1 and Morse et al. 1998), corresponds to the relevant speed of sound multiplied by the time elapsed since the Great Eruption. The observed characteristic scale size is larger, but does not contradict this basic idea: that the clumpy (“granular”) small-scale structure in each bipolar lobe represents features in the eruptive wind that were frozen into the freely expanding ejecta. Given the quantitative details mentioned above, the corrugated structures probably did *not* result from an instability in the flow long after the eruption (Kelvin-Helmholtz, Rayleigh-Taylor-like, or their kin). The structure, which pictorially resembles solar granulation, may have resulted from wind instabilities or from effects near the stellar surface (the sonic point). According to Shaviv (2000), porous structure should develop in a super-Eddington wind like that of η Car during 1838–1858. This porosity may be imprinted in clumps or holes seen in the polar lobes, and may prove more useful than the large-scale lobe shapes for understanding the Great Eruption itself.

5.6. Related Problems

The proposed wind structure with high ionization at low latitudes and dense optically-thick low-ionization zones near the poles helps explain several peculiarities:

1. High-ionization [Ne III] and [Fe III] emission regions exist a few hundred AU from the star even though the dense wind is expected to absorb the star’s ionizing photons (e.g., see model in Hillier et al. 2001). This is one motivation for the binary hypothesis, wherein a second star can provide ionizing radiation. However, the non-spherical wind that we propose may allow UV photons to escape from the primary star at low latitudes. This occurs despite gravity darkening at the stellar surface; the wind is opaque near the poles but semi-transparent at low latitudes. The “Weigelt blobs,” bright emission-line sources northwest of the star, are indeed thought to be located near the equatorial plane (Davidson et al. 1995, 1997).
2. The brightness of the Weigelt blobs is also a problem, since they seem to reflect more of the star’s light than they intercept, for their presumed size (see Davidson & Humpherys 1986). Dust is continually forming in η Car’s wind, evidenced by the unresolved hot dust in the core of the Homunculus seen in infrared images (e.g., Smith et al. 1998, 2002). If dust forms primarily in dense polar regions of the wind, it might help obscure the star along our line of sight more than toward the Weigelt blobs.
3. The simultaneous existence of separate high- and low-excitation regions in the wind helps explain the range of spectral types from B2 to B8 Ia seen in the far-UV spectrum of η Car by Ebbets et al. (1997).
4. The spherical wind model used by Hillier et al. (2001) overestimates the depth of the P Cygni absorption components in Balmer and Fe II lines. Figures 4 and 10 show that both species show deeper absorption in reflected spectra from the SE lobe than in our direct line of sight to the star. This supports the hypothesis (point number 2 above) that dense polar zones of η Car’s wind dominate the optical spectrum,

and the spherical model used by Hillier et al. more closely approximates polar wind conditions.

5. In addition to the Weigelt blobs, extended *equatorial* ejecta around η Car show peculiar excitation that might be less mysterious if η Car has a stronger UV flux at low latitudes. Equatorial regions would also see enhanced Ly α emission escaping from the polar wind, relevant to some proposed excitation mechanisms (Johansson & Hamann 1993; Hamann et al. 1999). Notable extended equatorial features are the “purple haze” in *HST* images (Morse et al. 1998), gas in the inner torus seen in infrared and optical images (Smith et al. 1998, 2002), the bizarre Fe II lines near ~ 2507 Å (see Davidson et al. 1995, 1997; Johansson et al. 1998; Hamann et al. 1999; Johansson & Letokhov 2001), and other Fe II and metal lines in the equatorial skirt with strange velocities and excitation (Zethson et al. 1999). Extended equatorial gas in the circumstellar torus also shows peculiar *variability* (Duncan et al. 1995; Smith et al. 2000; Smith & Gehrz 2000), which may be related to spectroscopic changes discussed below.

6. TEMPORAL VARIABILITY

So far we have discussed the wind during its normal high-excitation state as observed in March 2000, but η Car also has occasional “spectroscopic events” in which the spectrum temporarily changes for reasons that are not yet understood. Originally these events were interpreted as single-star shell ejections (Zanella, Wolf, & Stahl 1984; Bidelman et al. 1993), but a companion star seems likely, given the 5.5-year periodicity associated with the events (Damineli 1996; Whitelock et al. 1994; Corcoran et al. 1995; Duncan et al. 1995; Damineli et al. 1997, 1998; Davidson 1999).

Limited HST/STIS data were obtained during the most recent spectroscopic event in 1997–98 and at a few later times. Davidson et al. (1999) described some results for the star viewed directly, and remarked that the spectroscopic changes resembled a shell ejection (see also Gull et al. 1999; Davidson 1999, 2001). We can apply the same latitude-dependent reflection method described above to the March 1998 and February 1999 STIS data, where H α and He I $\lambda 6680$ were sampled with long exposure times on a particular slit orientation and placement shown in Figure 1. Unfortunately this slit position was not the same as for the March 2000 observations discussed above, but it crossed the Homunculus in a similar way. Here we describe significant changes in the reflected spectra; a report on the directly-viewed star is in preparation (Davidson et al.).

6.1. He I Variability

Figure 12 shows grayscale representations of long-slit spectra for He I $\lambda 6680$ in March 1998 and February 1999, and Figure 13 demonstrates variability of He I line profiles with tracings of the central star, as well as reflected spectra from the NW and SE lobes. Equivalent widths measured for these tracings are plotted in Figure 14. At positions in the NW polar lobe, He I $\lambda 6680$ is absent in March 1998 and extremely weak in February 1999. Positions in the NW lobe during March 1998 reflect the spectrum of the star 1 to 3 months earlier (soon after the event), and show that this feature nearly vanished, at least at these low latitudes. STIS spectra of the central star during the event in late December 1997 show that the He I $\lambda 6680$ flux remained detectable along our direct line of sight (Figure 13). In the SE polar lobe the equivalent width in Figure 14 is nearly constant. Also, in March 1998 the He I emission line in the SE lobe is stronger than it is in the NW polar lobe almost a year later in February 1999. This could not be the case if changes in the He I line were spherically symmetric (the time delay for positions in the SE lobe is only a few weeks).

In §4 we noted that the SE lobe in March 2000 showed a broad, roughly symmetric stellar-wind He I profile, plus reflected narrow emission from slow-moving inner ejecta such as the Weigelt blobs. The narrow line disappeared during 1998 and early 1999; compare Figure 12 to Figure 2. Meanwhile, as shown in Figure 13, the polar view of the stellar wind component (“SE lobe”) changed in a way quite unlike that observed directly on the star. The latitude dependence of He I variability probably indicates that *the wind’s asphericity was changing* during and after the 1997–98 event. Figure 14 shows that broad He I emission faded mainly at low latitudes, while the polar wind seemed relatively undisturbed.

6.2. H α Variability

H α emission seen directly in the spectrum of the central star has remained roughly constant in brightness relative to the continuum and in width, but its P Cyg absorption changed during 1998–99 (see Davidson et al. 1999; Davidson 2001). Changes in the latitudinal dependence of reflected P Cygni absorption are striking (Figure 12); tracings of the H α line are shown in Figures 15 and 16, and corresponding velocities are listed in Table 2. In our direct view of the star, deep P Cyg absorption around -520 km s $^{-1}$ occurred in early 1998 during the event but virtually disappeared before February 1999. Meanwhile, however, strong P Cyg absorption persisted at high latitudes, and its extreme velocity grew from -650 km s $^{-1}$ in 1998 to -1000 km s $^{-1}$ in 2000 (SE lobe, Figures 15 & 16). Deep P Cyg absorption seen at low latitudes in March 1998 disappeared two years later.

Thus, viewing the spectra seen in early 1998 rather than 2000, we realize that *the strong latitude dependence described in §5 above did not apply during the 1997–98 spectroscopic event*. At that time the depth of the P Cyg absorption was less latitude-dependent, while the extreme observed speeds that we have denoted $|v_\infty|$ temporarily decreased at high latitudes but increased at low latitudes (Figure 17). The wind was evidently disrupted through a wide latitude range, most likely by a “shell ejection” that increased the density especially at low latitudes. This may help to explain why Hillier et al. (2001) could reproduce the early-1998 spectrum fairly well with a spherical wind model, but found later spectra more problematic.

6.3. Implications for the Wind Geometry

In two ways the temporal variability appears very consistent with the hypothetical bipolar wind geometry sketched in Figure 11 (§5). First, a moderate shell ejection can easily decrease the ionization in the low-latitude wind, but should have less effect on the polar wind which is normally denser and less ionized. Qualitatively, at least, the observed behavior matched this expectation. Second, the 1998–99 temporary disappearance of the highest observable velocities (~ 1000 km s $^{-1}$, Figure 5) suggests that the fast material occurs in the polar wind *per se* within $0.5''$ of the star, and not at larger radii in the Homunculus lobes. Our reason for saying this is that the recombination time $(\alpha_B n_e)^{-1}$ is too long for rapid response, i.e., longer than a year, at radii more than a few hundred AU from the star.

Finally, we note that if the March 2000 data – midway through the 5.5-year spectroscopic cycle – represent the “normal” state, then Figures 16 and 17 indicate that the post-event recovery extended over more than a year. This is not what one would expect in a simple binary model, since the hypothetical companion star should have moved a considerable distance, ~ 10 AU, from the primary in less than 6 months after periastron passage (see, e.g., Davidson 1999).

7. IMPLICATIONS FOR THE 5.5 YR SPECTROSCOPIC CYCLE AND A MORE LIMITED ROLE FOR THE HYPOTHETICAL COMPANION STAR

The results discussed above suggest that the 1997–98 spectroscopic event was essentially a disturbance of the primary wind, and not, for instance, an eclipse or occultation. Most likely the term “shell ejection” is valid to some extent, as advocated by Zanella et al. (1984), Davidson (1999), and Davidson et al. (1999). None of the observations directly requires a companion star; a single-star model remains conceivable, but a binary model is not precluded either. Here, largely independent of whether the system is a binary, we describe a qualitative scenario for a spectroscopic event with the observed latitude dependences, and we list a variety of ways in which it appears consistent with observations. We assume that stronger hydrogen P Cygni absorption implies higher local mass density as discussed in §5; other interpretations may exist but would be more complicated. Detailed calculations are obviously needed but will be quite difficult, since a proper model must be two- or three-dimensional, with continuum- and line-driven gas dynamics, rotation, realistic NLTE level populations and radiative transfer, etc.

7.1. A Shell Ejection During the Spectroscopic Event

Figure 18 shows the likely arrangement of zones in η Car’s wind at three sample times: before, during, and soon after a spectroscopic event. This is merely a schematic diagram, and boundaries between zones are not necessarily sharp. Figure 18a usually applies: ionizing UV can escape through the lower-density low-latitude regions as conjectured in §5. Then, during an event (Figure 18b), the low-latitude wind becomes denser, mostly non-ionized, and opaque to ionizing photons. A density-increase factor of the order of 2 may suffice and the extra mass ejected might be as little as $2 \times 10^{-5} M_{\odot}$. Meanwhile, a relatively weaker high-latitude increase has less effect on the emergent spectrum; lessened values of v_{∞} and v_{pcyg} shown in Figures 16 and 17 may indicate that hydrogen recombines closer to the star, or that the polar wind slows as its mass increases. A few months later (Figure 18c), the ejected “shell” gradually becomes transparent. Altogether this scheme, where changing density at low latitudes acts as a sort of *valve* regulating the escape of UV photons, can account for nearly all observed characteristics of each spectroscopic event:

1. Narrow [Ne III], [Fe III], He I, and related emission lines temporarily fade – the phenomenon that led Zanella et al. (1984) to propose a UV-quashing “shell ejection.” We now know that these features originate in slow-moving *low-latitude* ejecta close to the star (Davidson et al. 1995, 1997; Smith et al. 2000).
2. Broad He I emission lines weaken during an event (Damineli 1996; Damineli et al. 1997, 1998). These probably originate in low-latitude wind zones (§6.1).
3. Broad (i.e., wind) components of some low-excitation lines such as Fe II become stronger (Damineli et al. 1998). This is qualitatively unsurprising if the volume and mass of low-excitation material increase as the wind becomes quasi-spherical (Figure 18b).
4. In our direct view of the star, many violet and UV absorption features deepen during an event, reminiscent of a shell ejection (Davidson et al. 1999).
5. In the time period between spectroscopic events, colliding-wind X-ray binary models for η Car (Ishibashi et al. 1999; Corcoran et al. 2001; Pittard & Corcoran 2002) seem to require a primary mass-loss rate of only a few times $10^{-4} M_{\odot} \text{ yr}^{-1}$, a factor of three to ten less than the familiar value based on other considerations (Hillier et al. 2001; Davidson & Humphreys 1997). However, if the primary wind is not spherical in its “normal” state, then the X-ray parameters refer mainly to local densities around the shock

interface, presumably within the low-latitude, lower density part of the primary wind sketched in Figure 18a. Corcoran et al. (2001) also invoke a sudden density increase to explain the collapse of the X-ray flux during an event, which seems consistent with the shell-ejection scenario depicted in Figure 18.

6. The radio-wavelength behavior of η Car includes varying free-free emission near the equatorial plane (Duncan et al. 1995). The source is compact during an event, and later expands irregularly as ionizing photons penetrate to larger distances from the star. Near-infrared images, also representing free-free continuum emission mostly at low latitudes, show changes morphologically similar to the radio emission (Smith & Gehrz 2000).

7. The 7 mm flux, produced by free-free emission in outer parts of the wind, fades during a spectroscopic event (Abraham & Damineli 1999). This can be explained if some normally ionized (low-latitude) portions of the wind recombine during the event. (Millimeter-wavelength continuum mostly originates within 100 AU of the star, while centimeter wavelengths mentioned above in point 6 represent ejecta farther out.)

8. The variable geometry and emitting volume of the wind may cause serious line profile variations like those that are observed. As noted by McGregor et al. (1999) and Davidson et al. (2000), this makes it difficult or impossible to correlate radial velocities with possible orbital motion.

9. There is almost no obvious large-scale photoionization in the high-latitude zones around the star; the [Ne III] and similar features mentioned in point 1 above appear to be fairly close to the equatorial plane based on their Doppler velocities, and so is the centimeter-wavelength emission mentioned in point 6. Since there is no shortage of gas at various radii within the Homunculus lobes (see Ishibashi et al. 2001), we conclude that ionizing UV photons are scarce at high latitudes. This may be an objection to the most likely type of binary model, wherein a hot companion star produces ionizing radiation. Since the primary wind does not seem dense enough to block ionizing photons at the hypothetical apoastron distance (~ 30 AU), we should expect to see bright photoionized material in near-polar locations around the star, contrary to observations. The single-star geometry sketched in Figure 18a, on the other hand, can emit ionizing radiation toward low latitudes only, consistent with the observed large-scale ionization.

7.2. Rotation and a Companion Star's Influence

In most binary schemes for η Car's 5.5-year cycle (e.g., Damineli et al. 1997, 2000; and various authors in Morse et al. 1999), a hot companion star in an eccentric orbit is the main perpetrator. It provides a fast wind needed for the X-rays, and – far greater in the energy budget – it supplies ionizing UV radiation to excite emission lines in surrounding ejecta. Emergent UV and X-rays are modulated by the secondary star's varying radial location in the dense primary wind. In the latitude-dependent shell ejection scenario that we propose, however, much (perhaps nearly all) of the UV radiation comes from the primary rather than the secondary star. A companion star may still be needed for the hard X-rays from η Car (Corcoran et al. 1998, 2001; Ishibashi et al. 1999; Ishibashi 2001; Pittard & Corcoran 2002; etc.), but at wavelengths other than X-rays – i.e., for 99.99% of the energy flow – the main role of a hypothetical secondary star is to regulate the periodicity. It may supply the most extreme UV photons, but this is unproven.

Most likely a spectroscopic event occurs near periastron passage when the secondary star tidally disturbs the surface layers of an already unstable primary. This is feasible, at a separation more than 3 times the primary's radius, only because radiation pressure and (probably) rotation magnify the tidal effect. In §5.3 we noted how η Car's wind geometry qualitatively matches theoretical predictions by Owocki et al. (1996)

for a rotating star with gravity darkening. In that formulation, gravity darkening followed $F \propto g_{eff}$ (von Zeipel 1924), and simple scaling arguments would lead to $v_\infty \propto T^2$. This is probably an oversimplification for η Car’s optically-thick wind, but the agreement between the observed wind structure and the associated predictions from theory suggest that it is not too far-fetched. Therefore, the pole-to-equator velocity ratio of ~ 2 (Figure 7) during the normal high-excitation state implies, very crudely, that $T_{pole}/T_{equator} \approx \sqrt{2}$. Thus, if η Car’s polar temperature is close to the often-adopted value of 30,000 K (e.g., Davidson & Humphreys 1997; Hillier et al. 2001), then the corresponding temperature at low latitudes could be dangerously close to 21,000 K, where an important opacity increase toward lower temperatures occurs (see Pauldrach & Puls 1990; Lamers & Pauldrach 1991). Intuition then guides us to ask: What happens if the rotation rate is slightly increased? Such a change should increase the amount of gravity darkening, decrease T , and raise opacity at the equator — i.e. rotation may trigger an equatorial shell ejection.

The rotation in question may be innate or it may have been forced by a companion star, but either way the bipolar Homunculus strongly suggests that rotation is indeed significant in η Car. Thus we conjecture that *systematic variations of the surface rotation rate play a role in η Car’s 5.5-year cycle*. The reasoning, mentioned earlier by Davidson (1999), goes like this:

1. Imagine, for simplicity, that η Car initially has solid-body rotation, with a constant angular rate Ω . (This assumption merely makes the next two steps easier to visualize.)
2. Then any surface eruption carries away a larger-than-average angular momentum per unit mass.
3. Afterward, the star very quickly readjusts to a new state of quasi-hydrostatic equilibrium. The dense inner region containing most of the mass is scarcely affected, but the outermost surviving layers must expand appreciably outward and therefore now have slower rotation rates.
4. At this point the star’s dense center rotates faster than the less massive outer layers. Therefore angular momentum will diffuse outward, gradually accelerating the surface rotation. According to simple order-of-magnitude turbulent diffusion estimates, a spin-up timescale of a few years seems plausible following the ejection of less than $10^{-3} M_\odot$.
5. Thus we conjecture that the surface rotation rate gradually increases during the 5.5-year period, with possible effects on the low-latitude temperature (gravity darkening), on the wind, etc. Rotation is always far slower than the naive “break-up” limit, but toward the end of the cycle it may be fast enough to have a destabilizing effect as noted earlier. Internal thermal readjustment can meanwhile play a related role.
6. Most likely this development affects a binary model, and tidal friction near periastron may play a long-term role. However, one can also imagine a *single-star* cycle based on the above reasoning. In such a model, 5.5 years is the time required for spin-up to permit another mass ejection event. There is no obvious physical reason why such a periodicity cannot be as regular as the observed cycle. Other single-star alternatives for short-term periodicity exist as well (e.g., Stothers 2000; Guzik et al. 1999; Davidson 1999). These could act independently, or they could be assisted or regularized by interactions with a companion.

The wind geometry, shaped by rotation and/or a companion star, may also affect long-term spectroscopic variations. Feast et al. (2001) found in old spectrograms that η Car was continuously in a low-excitation (“event”) state for many years before 1920. Most likely the wind was then quasi-spherical as in Figure 18b. The large amount of mass ejected in η Car’s 19th century eruptions (see Humphreys et al. 1999) represented most of the star’s prior radius, so we *expect* the surface of η Car to have been rotating very slowly a century ago. Without rotation, there was no reason for the wind to have the modern non-spherical shape shown in Figure 18a; in particular there would not have been a lower-density zone near the equatorial plane which

today allows UV photons to escape. Therefore, no matter whether the hard UV comes from the primary or from a secondary star, such radiation could have been absorbed within the dense primary wind at low latitudes – hence no high-excitation emission lines then. Later, we must suppose, the surface rotation rate gradually increased for the reason noted above, until it became sufficient to establish the current geometry and high-excitation spectrum sometime around 1940 when a sudden brightening occurred (de Vaucouleurs & Eggen 1952; Thackeray 1953; Gaviola 1953). This coincidence suggests that the presence of spectroscopic events is linked to changes in the primary star, which dominates the observed optical flux.

Although η Car is an extreme case, rotation-induced wind structure and angular momentum diffusion may play important roles for mass ejections from other Luminous Blue Variables. This is not a new revelation, but our latitude-dependent study of η Car suggests the possibilities quite vividly.

The authors benefitted from interesting and informative conversations with Stan Owocki, Joe Cassinelli, and Roberta Humphreys. An anonymous referee gave several suggestions that improved the presentation of the paper. N.S. is grateful for the support of a NASA/GSRP fellowship from Goddard Space Flight Center. Additional support was provided by NASA through grant number GO-8327 (P.I.: Davidson) from the Space Telescope Science Institute, which is operated by the Association for Research in Astronomy, Inc., under NASA contract NAS 5-26555, and through STIS GTO resources and funding (P.I.: Gull).

REFERENCES

Abraham, Z., & Damineli, A. 1999, in ASP Conf. Ser. 179, Eta Carinae at the Millenium, ed. J.A. Morse, R.M. Humphreys, & A. Damineli (San Francisco: ASP), 263

Balick, B., & Matt, S. 2001, in ASP Conf. Ser. 242, Eta Carinae and Other Mysterious Stars, ed. T. Gull, S. Johansson, & K. Davidson (San Francisco: ASP), 155

Bidelman, W.P., Galen, T.A., & Wallerstein, G. 1993, PASP, 105, 785

Bjorkman, J.E., & Cassinelli, J.P. 1993, ApJ, 409, 429

Castor, J.I., Abbott, D.C., & Klein, R.I. 1975, ApJ, 195, 157

Cranmer, S.R., & Owocki, S.P. 1995, ApJ, 440, 308

Corcoran, M.F., Rawley, G.L., Swank, J.H., & Petre, R. 1995, ApJ, 445, L121

Corcoran, M.F., et al. 1998, ApJ, 494, 381

Corcoran, M.F., Ishibashi, K., Swank, J.H., & Petre, R. 2001, ApJ, 547, 1034

Currie, D.G., et al. 1996, AJ, 112, 1115

Damineli, A. 1996, ApJ, 460, L49

Damineli, A., Conti, P.S., & Lopes, D.F. 1997, New Astron., 2, 107

Damineli, A., Stahl, O., Kaufer, A., Wolf, B., Quast, G., & Lopes, D.F. 1998, A&A SS, 133, 299

Damineli, A., Kaufer, A., Wolf, B., Stahl, O., Lopes, D.F., & de Araujo, F.X. 2000, ApJ, 528, L101

Davidson, K. 1999, in ASP Conf. Ser. 179, Eta Carinae at the Millenium, ed. J.A. Morse, R.M. Humphreys, & A. Damineli (San Francisco: ASP), 304; see also p. 374

Davidson, K., 2001, in ASP Conf. Ser. 242, Eta Carinae and Other Mysterious Stars, ed. T. Gull, S. Johansson, & K. Davidson (San Francisco: ASP), 3

Davidson, K., & Humphreys, R.M. 1986, A&A, 164, L7

Davidson, K., & Humphreys, R.M. 1997, ARAA, 35, 1

Davidson, K., Dufour, R.J., Walborn, N.R., & Gull, T.R. 1986, ApJ, 305, 867

Davidson, K., Ebbets, D., Weigelt, G., Humphreys, R.M., Hajian, A., Walborn, N.R., & Rosa, M. 1995, AJ, 109, 1784

Davidson, K., Ebbets, D., Johansson, S., Morse, J.A., Hamann, F.W., Balick, B., Humphreys, R.M., Weigelt, G., & Frank, A. 1997, AJ, 113, 335

Davidson, K., Ishibashi, K., Gull, T.R., & Humphreys, R.M. 1999, in ASP Conf. Ser. 179, Eta Carinae at the Millenium, ed. J.A. Morse, R.M. Humphreys, & A. Damineli (San Francisco: ASP), 227

Davidson, K., Ishibashi, K., Gull, T.R., Humphreys, R.M., & Smith, N. 2000, ApJ, 530, L107

Davidson, K., Smith, N., Gull, T.R., Ishibashi, K., & Hillier, D.J. 2001, AJ, 121, 1569

de Vaucouleurs, G., & Eggen, O.C. 1952, PASP, 64, 185

Duncan, R.A., White, S.M., Nelson, G.J., Drake, S.A., & Kundu, M.R. 1995, *ApJ*, 441, L73

Dwarkadas, V.V., & Balick, B. 1998, *AJ*, 116, 829

Dwarkadas, V.V., & Owocki, S.P. 2002, preprint

Ebbets, D.C., Walborn, N.R., & Parker, J.W. 1997, *ApJ*, 489, L161

Eddington, A.S. 1926, *The Internal Constitution of the Stars*, sections 198–200

Feast, M., Whitelock, P., & Marang, F. 2001, *MNRAS*, 322, 741

Frank, A., Balick, B., & Davidson, K. 1995, *ApJ*, 441, L77

Frank, A., Ryu, D., & Davidson, K. 1998, *ApJ*, 500, 291

Friend, D.B., & Abbott, D.C. 1986, *ApJ*, 311, 701

Gaviola, E. 1953, *ApJ*, 118, 234

Glatzel, W. 1998, *A&A*, 339, L5

Gull, T.R., Ishibashi, K., Davidson, K., and the Cycle 7 STIS GO Team, 1999, in *ASP Conf. Ser.* 179, *Eta Carinae at the Millenium*, ed. J.A. Morse, R.M. Humphreys, & A. Damineli (San Francisco: ASP), 144

Gull, T.R., & Ishibashi, K. 2001, in *ASP Conf. Ser.* 242, *Eta Carinae and Other Mysterious Stars*, ed. T. Gull, S. Johansson, & K. Davidson (San Francisco: ASP), 59

Guzik, J.A., Cox, A.N., & Despain, K.M. 1999, in *ASP Conf. Ser.* 179, *Eta Carinae at the Millenium*, ed. J.A. Morse, R.M. Humphreys, & A. Damineli (San Francisco: ASP), 347

Hamann, F., DePoy, D.L., Johansson, S., & Elias, J. 1994, *ApJ*, 422, 626

Hamann, F., Davidson, K., Ishibashi, K., & Gull, T.R. 1999, in *ASP Conf. Ser.* 179, *Eta Carinae at the Millenium*, ed. J.A. Morse, R.M. Humphreys, & A. Damineli (San Francisco: ASP), 116

Hillier, D.J., & Allen, D.A. 1992, *A&A*, 262, 153

Hillier, D.J., Davidson, K., Ishibashi, K., & Gull, T.R. 2001, *ApJ*, 553, 837

Humphreys, R.M., Davidson, K., & Smith, N. 1999, *PASP*, 111, 1124

Ignace, R., Cassinelli, J.P., & Bjorkman, J.E. 1996, *ApJ*, 459, 671

Ishibashi, K., Corcoran, M.F., Davidson, K., Swank, J.H., Petre, R., Drake, S.A., Damineli, A., & White, S. 1999, *ApJ*, 524, 983

Ishibashi, K. 1999, in *ASP Conf. Ser.* 242, *Eta Carinae and Other Mysterious Stars*, ed. T. Gull, S. Johansson, & K. Davidson (San Francisco: ASP), 53

Ishibashi, K., Gull, T.R., & Davidson, K. 2001, in *ASP Conf. Ser.* 242, *Eta Carinae and Other Mysterious Stars*, ed. T. Gull, S. Johansson, & K. Davidson (San Francisco: ASP), 71

Johansson, S., & Hamann, F. 1993, *Physica Scripta*, T47, 157

Johansson, S., Leckrone, D.S., & Davidson, K. 1998, in *ASP Conf. Ser.* 143, *The Scientific Impact of the GHRS*, ed. J.C. Brandt, C.C. Petersen, & T.B. Ake (San Francisco: ASP), 155

Johansson, S., & Letokhov, V.S. 2001, *A&A*, 378, 266

Kippenhahn, R., & Weigert, A. 1990, *Stellar Structure and Evolution* (Berlin: Springer-Verlag), section 42.2

Langer, N., Garcia-Segura, G., & Mac Low, M.M. 1999, *ApJ*, 520, L49

Lamers, H.J.G.L.M., & Pauldrach, A.W.A. 1991, *A&A*, 244, L5

Lamers, H.J.G.L.M., & Cassinelli, J.P. 1999, “Introduction to Stellar Winds” (Cambridge: Cambridge University Press)

Lee, U., Saio, H., & Osaki, Y. 1991, *MNRAS*, 250, 432

López, J.A., & Meaburn, J. 1986, *RevMexAA*, 13, 27

Maeder, A. 1999, *A&A*, 347, 185

Maeder, A., & Desjacques, V. 2001, *A&A*, 372, L9

Maeder, A., & Meynet, G. 2000, *A&A*, 361, 159

McGregor, P.J., Rathborne, J.M., & Humphreys, R.M. 1999, in *ASP Conf. Ser.* 179, *Eta Carinae at the Millenium*, ed. J.A. Morse, R.M. Humphreys, & A. Damineli (San Francisco: ASP), 236

Meaburn, J., Wolstencroft, R.D., & Walsh, J.R. 1987, *A&A*, 181, 333

Meaburn, J., Gehring, G., Walsh, J.R., Palmer, J.W., Lopez, J.A., Bruce, M., & Raga, A.C. 1993, *A&A*, 276, L21

Morse, J.A., Davidson, K., Bally, J., Ebbets, D., Balick, B., & Frank, A. 1998, *AJ*, 116, 2443

Morse, J.A., Humphreys, R.M., & Damineli, A. (eds.) 1999, *ASP Conf. Ser.* 179, *Eta Carinae at the Millenium* (San Francisco: ASP)

Morse, J.A., Kellogg, J.R., Bally, J., Davidson, K., Balick, B., & Ebbets, D. 2001, *ApJ*, 548, L207

Najarro, F., Hillier, J.D., & Stahl, O. 1997, *A&A*, 326, 1117

Owocki, S.P. 2002, private communication

Owocki, S.P., Cranmer, S.R., & Blondin, J.M. 1994, *ApJ*, 424, 887

Owocki, S.P., Cranmer, S.R., & Gayley, K.G. 1996, *ApJ*, 472, L115

Owocki, S.P., Gayley, K.G., & Cranmer, S.R. 1998, in *ASP Conf. Ser. 131, Boulder Munich II: Properties of Hot Luminous Stars*, ed. I.D. Howarth (San Francisco: ASP), 237

Owocki, S.P., & Gayley, K.G. 1997, in *ASP Conf. Ser. 120, Luminous Blue Variables: Massive Stars in Transition*, ed. A. Nota & H.J.G.L.M. Lamers (San Francisco: ASP), 121

Pauldrach, A.W.A., & Puls, J. 1990, *A&A*, 237, 409

Pittard, J.M., & Corcoran, M.F. 2002, *A&A*, 383, 636

Puls, J. 1996, *A&A*, 305, 171

Shaviv, N.J. 2000, *ApJ*, 532, L137

Smith, N., & Gehrz, R.D. 1998, *AJ*, 116, 823

Smith, N., Gehrz, R.D., & Krautter, J. 1998, *AJ*, 116, 1332

Smith, N., Gehrz, R.D., & Krautter, J. 1999, in *ASP Conf. Ser. 179, Eta Carinae at the Millenium*, ed. J.A. Morse, R.M. Humphreys, & A. Damineli (San Francisco: ASP), 31

Smith, N., & Gehrz, R.D. 2000, *ApJ*, 529, L99

Smith, N., Morse, J.A., Davidson, K., & Humphreys, R.M. 2000, *AJ*, 120, 920

Smith, N., & Davidson, K. 2001, *ApJ*, 551, L101

Smith, N. 2001, in *ASP Conf. Ser. 242, Eta Carinae and Other Mysterious Stars*, ed. T. Gull, S. Johansson, & K. Davidson (San Francisco: ASP), 81

Smith, N. 2002, *MNRAS*, 337, 1252

Smith, N., Gehrz, R.D., Hinz, P.M., Hoffmann, W.F., Mamajek, E.E., Meyer, M.R., & Hora, J.L. 2002, *ApJ*, 567, L77

Stothers, R.B. 2000, *ApJ*, 530, L103

Thackeray, A.D. 1953, *MNRAS*, 113, 237

Thackeray, A.D. 1961, *Observatory*, 81, 99

ud-Doula, A., & Owocki, S.P. 2002, preprint

Viotti, R., Rossi, L., Cassatella, A., Altamore, A., & Baratta, G.B. 1989, *ApJS*, 71, 983

Visvanathan, N. 1967, *MNRAS*, 135, 275

von Zeipel, H. 1924, *MNRAS*, 84, 665

Walborn, N.R., & Liller, M. 1977, *ApJ*, 211, 181

Washimi, H., & Shibata, S. 1993, *MNRAS*, 262, 936

White, S. 2002, private communication

Whitelock, P.A., Feast, M.W., Koen, C., Roberts, G., & Carter, B.S. 1994, *MNRAS*, 270, 364

Wolf, B., Kaufer, A., Stahl, O., & Damineli, A. 1999, in *ASP Conf. Ser. 179, Eta Carinae at the Millenium*, ed. J.A. Morse, R.M. Humphreys, & A. Damineli (San Francisco: ASP), 243

Wolf, B., Stahl, O., & Fullerton, A.W. (eds.) 1998, *Variable and Non-spherical Stellar Winds in Luminous Hot Stars* (Heidelberg: Springer)

Zanella, R., Wolf, B., & Stahl, O. 1984, *A&A*, 137, 79

Zethson, T., Johansson, S., Davidson, K., Humphreys, R.M., Ishibashi, K., & Ebbets, D. 1999, *A&A*, 344, 211

Zickgraf, F.J., Wolf, B., Leitherer, C., Appenzeller, I., & Stahl, O. 1986, *A&A*, 163, 119

Table 1: Measured parameters for H α in STIS spectra (March 2000)^a

Position (arcsec)	Width (arcsec)	Δv km s $^{-1}$	Latitude (deg)	v_∞ km s $^{-1}$	v_{pcyg} km s $^{-1}$	Comments
+7.3	0.44	785	53	-560	-435	NW lobe
+5.4	0.57	500	45	-475	-410 ^c	NW lobe
+3.3	1.00	350	35	...	-210 ^b	fan, no P Cyg abs.
+2.6	0.38	220	28	...	-150 ^b	fan, no P Cyg abs.
star	0.15	0	49	-540	-410 ^c	central star
-1.0	0.51	70	56	-640	-430 ^c	SE lobe
-1.5	0.33	105	61	-630	-450 ^c	SE lobe
-2.5	0.63	60	66	-700	-460 ^c	SE lobe, shadow
-3.0	0.38	100	69	-760	-480	SE lobe
-3.8	0.38	125	73	-780	-480	SE lobe
-4.3	0.38	125	77	-875	-480	SE lobe
-5.2	0.38	165	83	-1000	-550	SE lobe
-5.8	0.25	185	86	-1150	-590	SE lobe, polar axis
-7.0	0.51	270	82	-1050	-540	SE lobe
-8.0	0.38	350	74	-870	-460	SE lobe
NE 5 ^d	1.00	195	0	-750	-440	equatorial ejecta

^aSee text in §2 for a description of the various columns.

^bAt these offset positions, v_{pcyg} is the velocity of the narrow Balmer absorption seen in the NW lobe.

^cAt these offset positions, v_{pcyg} was measured for the H β line, since H α velocities are ambiguous due to contamination from [N II] emission. For H α and H β , v_∞ and v_{pcyg} were the same to within $\lesssim 10$ km s $^{-1}$ in March 2000.

^dThe spectrum of the NE5 offset position does not fully sample the 1'' \times 1'' box in Figure 1. Rather, adjacent slit positions were separated by 0''.25 intervals with a 52'' \times 0''.1 aperture oriented at P.A.=332 $^{\circ}$.1.

Table 2: Measured parameters for H α in STIS spectra (March 1998; February 1999)^a

Position (arcsec)	Width (arcsec)	Δv km s $^{-1}$	Latitude (deg)	v_∞ (1998) km s $^{-1}$	v_{pcyg} (1998) km s $^{-1}$	v_∞ (1999) km s $^{-1}$	v_{pcyg} (1999) km s $^{-1}$	Comments
+7.4	0.65	930	56	-660	-520	NW lobe
+6.0	1.84	710	49	-650	-500	-480	-360	NW lobe
+4.6	0.62	450	43	-300 ^b	NW lobe
+3.2	0.95	225	36	...	-170 ^b	...	-170 ^b	fan, no P Cyg abs.
+2.0	0.85	60	31	-750	-580	fan, no P Cyg abs.
star	0.15	0	49	-680	-520	-510 ^c	-460 ^c	central star
-1.1	0.29	70	55	-740	-590	SE lobe
-1.6	0.47	75	60	-850 ^c	-540	-580 ^c	-460	SE lobe
-2.3	0.55	75	64	-780 ^c	-550	...	-500 ^c	SE lobe
-2.9	0.70	90	67	-780 ^c	-540	...	-500 ^c	SE lobe
-3.8	0.57	100	71	-610	-480	-580	-460	SE lobe
-4.4	0.37	145	73	-640	-490	-640	-490	SE lobe
-5.0	0.49	165	76	-650	-500	-680	-500	SE lobe
-5.7	0.52	192	79	-640	-500	-690	-500	SE lobe
-6.9	0.52	270	78	-620	-480	-650	-480	SE lobe
-7.5	0.37	345	75	-590	-480	-580	-450	SE lobe
-7.9	0.39	400	72	-600	-480	-580	-460	SE lobe

^aSimilar to Table 1, but offset positions and latitudes differ here because of the slit orientation used (see Figure 1).

^bAt these offset positions, v_{pcyg} is the velocity of the narrow Balmer absorption seen in the NW lobe.

^cPoorly defined or contaminated by emission.

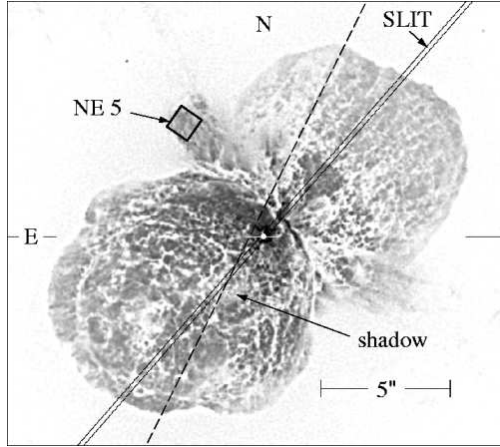


Fig. 1.— Orientation and size of the STIS slit used for the March 2000 observations. A second $1''$ square aperture located $5''$ NE of the star was used to extract the spectrum of one position in the equatorial ejecta. It is labeled “NE 5” and is discussed in §5.4. The dashed line shows the orientation of the $0''.1$ -wide slit used in March 1998 and February 1999 (see §6), which was intentionally offset from the star by $0''.4$. The dark spot labeled “shadow” is discussed in §4. The *HST*/WFPC2 image shown here was obtained in 1995 (see Morse et al. 1998), but its scale has been adjusted slightly to allow for expansion since then.

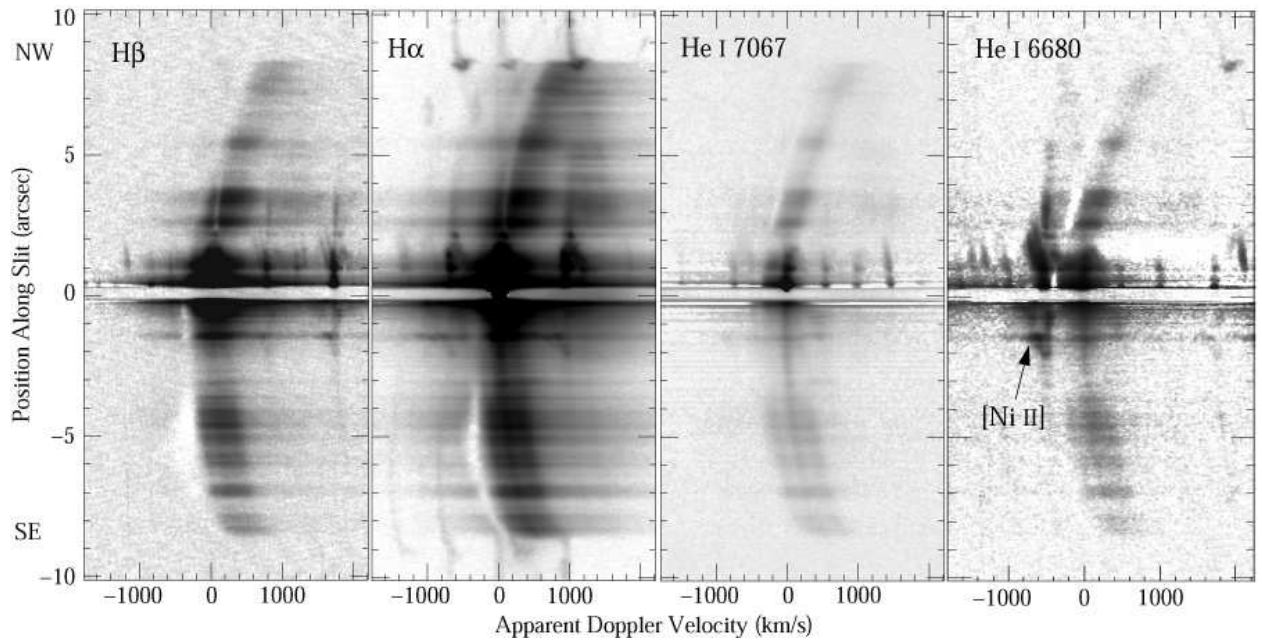


Fig. 2.— Continuum-subtracted long-slit STIS spectra (March 2000) of a few of the brightest reflected emission lines in η Car’s stellar wind, using the $0''.2$ -wide long-slit aperture shown in Figure 1.

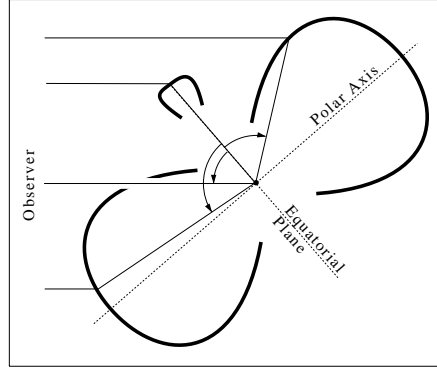


Fig. 3.— Schematic diagram showing the relationship between position and latitude for reflected light in the Homunculus Nebula. The vertical axis corresponds to distance along the slit and the horizontal axis is distance perpendicular to the plane of the sky. The thick curved lines represent the “compromise” shape for the reflecting surfaces of the bipolar lobes given by Davidson et al. (2001). The arrows designating angular measure refer to latitudes inferred for each line of sight.

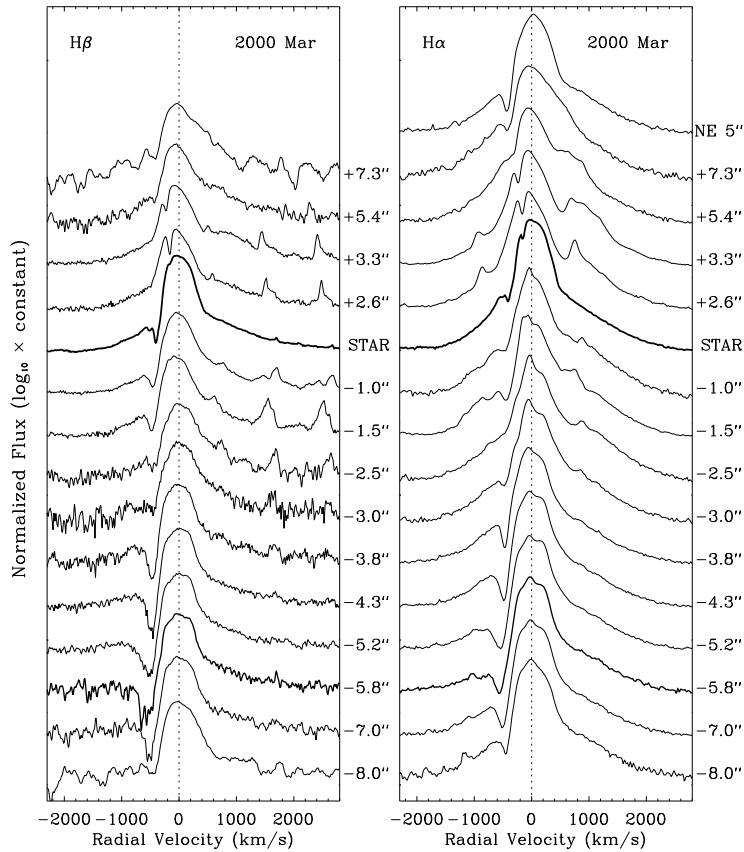


Fig. 4.— Tracings of several different positions along the slit for $H\beta$ and $H\alpha$, compared to the spectrum of the central star (shown with a thick solid line). Positional offsets for each line profile are indicated at the right side of each panel. The intensity scale is logarithmic. The narrow “notch” at -150 to -200 $km\ s^{-1}$ seen at a few positions in the NW lobe is probably not due to P Cyg absorption in the stellar wind, and will not be discussed in this paper. The tracing at $-5.^{\circ}8$ is the closest to the polar axis, and is drawn with a heavy line as well.

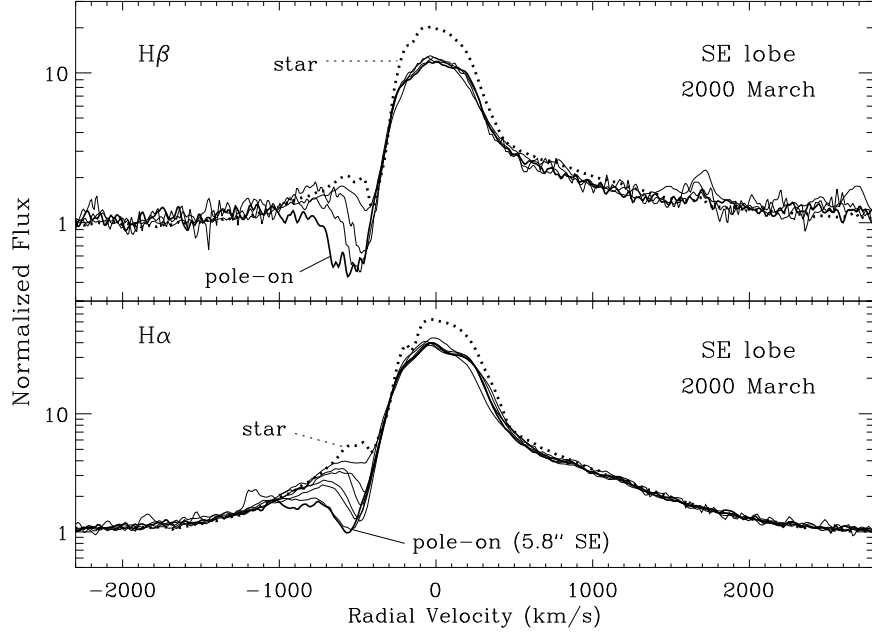


Fig. 5.— Tracings of $H\beta$ and $H\alpha$ line profiles from Figure 4 for selected positions in the SE lobe and central star, normalized to the same continuum level and superimposed on one another (log intensity scale). Again, the narrow “notch” at -140 km s^{-1} seen in the central star’s spectrum is probably not due to P Cyg absorption in the stellar wind, and will not be discussed in this paper. The star’s profile is taken from data obtained on 2000 March 20, as described in the text. These reflected profiles and those in other figures have been shifted horizontally by the corresponding value of Δv in Table 1 for each tracing.

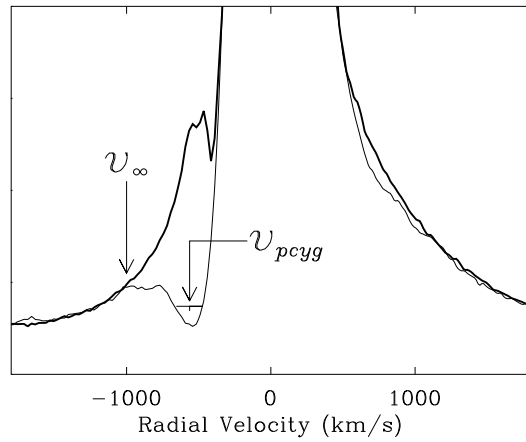


Fig. 6.— $H\alpha$ profiles of the star (heavy line) and one position in the SE lobe plotted on a linear intensity scale. The arrows indicate how we measured v_∞ and v_{pcyg} . v_{pcyg} is the mean between the slopes of the absorption trough at half-depth.

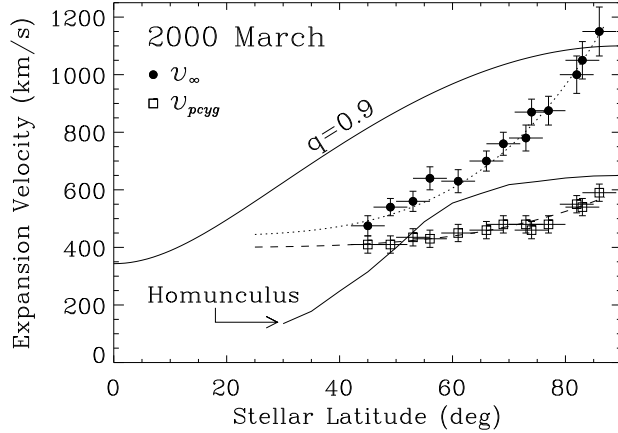


Fig. 7.— Variation of v_∞ and v_{pcyg} for the H α line as a function of stellar latitude in η Car's stellar wind. The solid line labeled “Homunculus” corresponds to the expansion velocities for the ‘compromise’ shape of the polar lobes presented by Davidson et al. (2001), if they were ejected in 1843. The other solid line is a curve for equation (1), with an arbitrary value of $q = 0.9$. The dotted and dashed lines show simple trends chosen for comparison with the plotted values of v_∞ and v_{pcyg} .

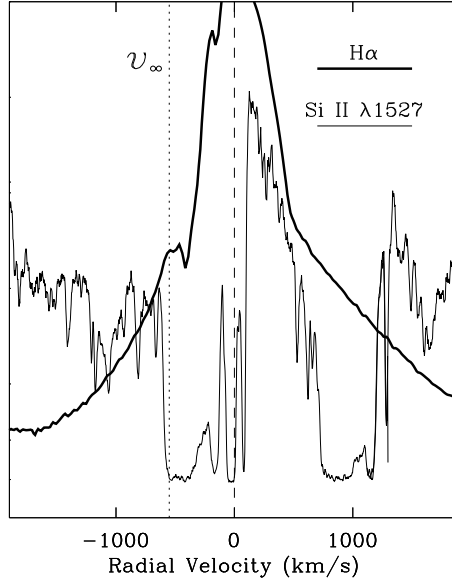


Fig. 8.— H α line profile of the central star (thicker line) observed on 20 March 2000, compared to the Si II $\lambda 1527$ line profile of the central star observed on 23 March 2000 with the STIS FUV/MAMA detector. Our method of measuring v_∞ in Balmer absorption profiles (dotted line) underestimates the true v_∞ (as measured in UV resonance lines) at a given latitude in the wind by less than ~ 50 km s^{-1} .

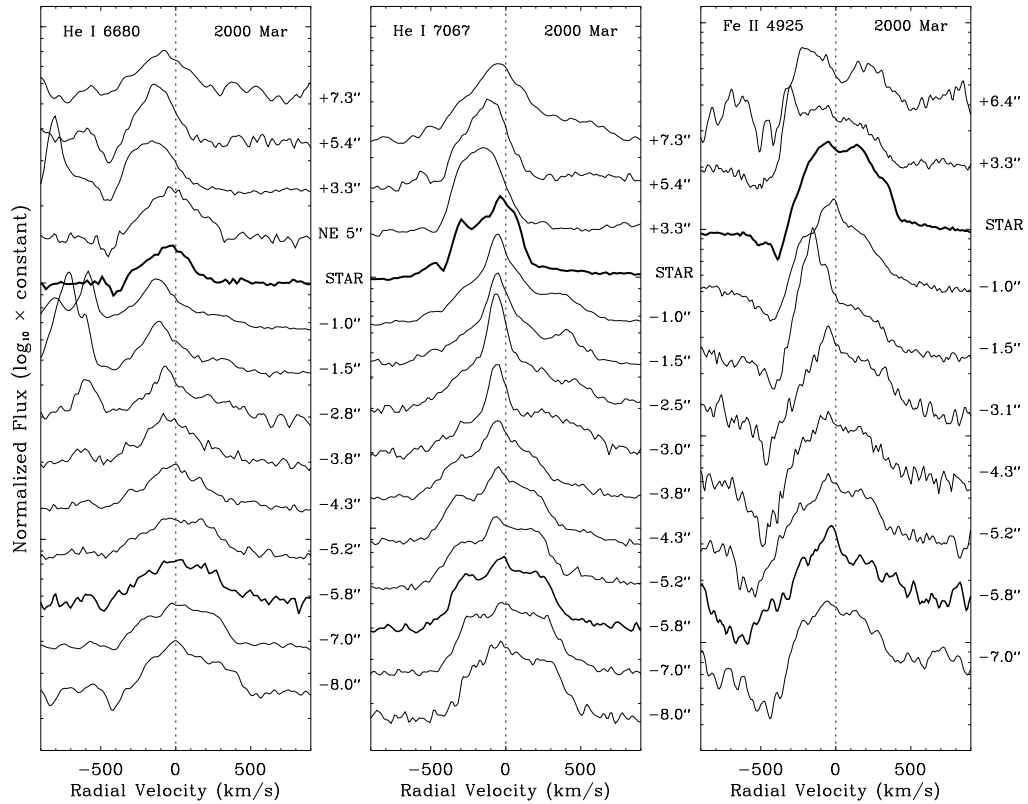


Fig. 9.— Tracings of several different positions along the slit for He I λ 6680 and λ 7067, and Fe II λ 4925, compared to the spectrum of the central star (shown by the thick solid line). Positional offsets for each line profile are indicated at the right side of each panel (log intensity scale). Again, the tracing at $-5.8''$ is the closest to the polar axis, and is drawn with a heavy line as well.

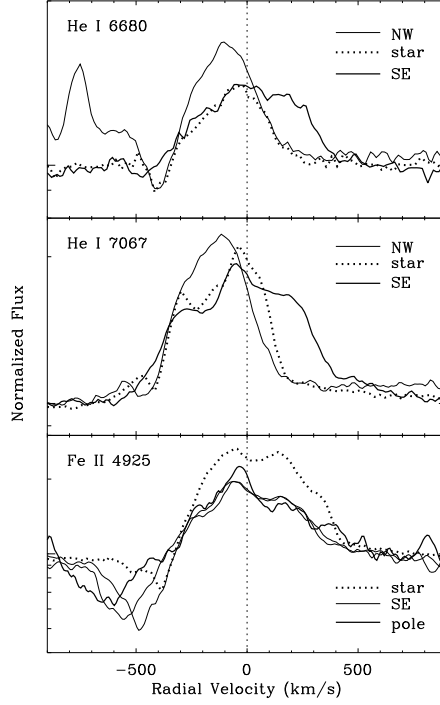


Fig. 10.— Selected tracings in March 2000 (some are averages of adjacent tracings) from Figure 6, normalized to the same continuum level and superimposed on one another (logarithmic intensity scale). “NW” and “SE” indicate the average reflected spectra from many positions in the NW or SE polar lobe. Tracings labeled “pole” are at $-5''8$ (see Table 1). The NW sample for Fe II $\lambda 4925$ is excluded because of contamination by narrow intrinsic emission. Extra He I $\lambda 6680$ emission at velocities between -900 and -500 is due to [Ni II] emission (see Figure 2).

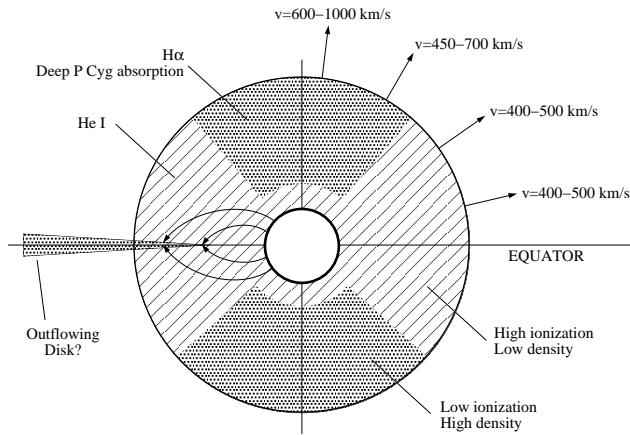


Fig. 11.— Cartoon model for latitudinal structure in η Car’s stellar wind during the normal high-excitation state in March 2000.

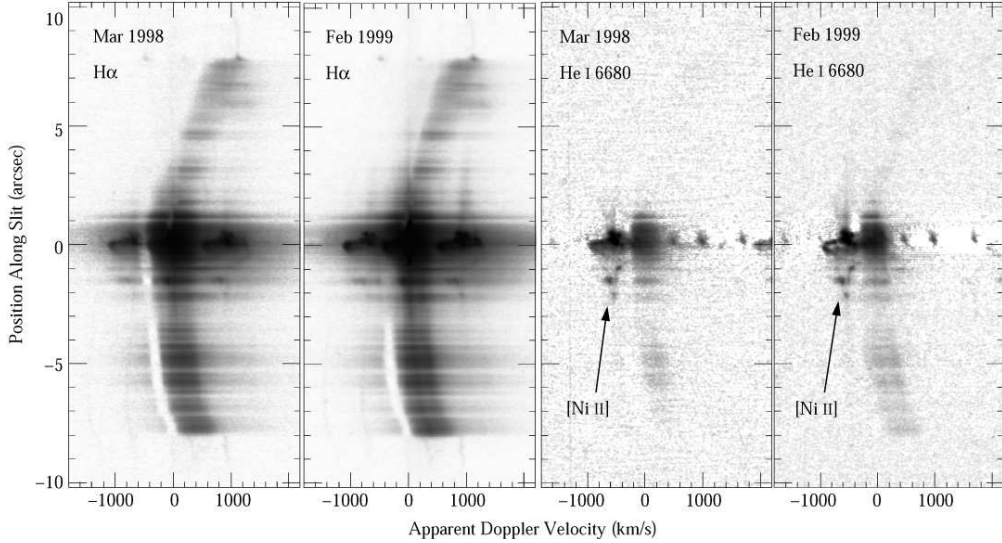


Fig. 12.— Continuum-subtracted long-slit spectra of $\text{H}\alpha$ and $\text{He I } \lambda 6680$ in March 1998 and February 1999. Compare with the same emission lines in March 2000 shown in Figure 2. Note, however, a slight difference in position angle and placement of the slit; these observations correspond to the dashed line in Figure 1.

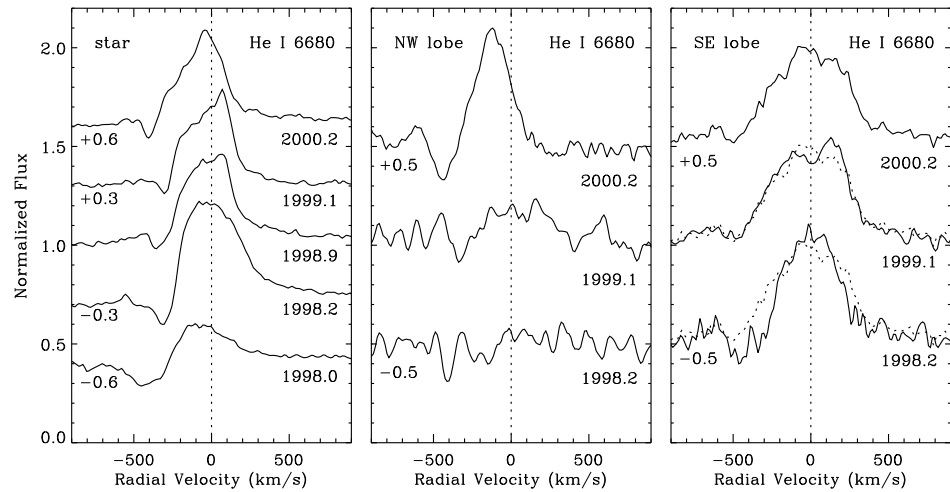


Fig. 13.— Variability of the $\text{He I } \lambda 6680$ line profile as seen directly at the position of the central star (left), in the NW polar lobe (center), and in the SE polar lobe (right). The tracing in the SE lobe for March 2000 is also superimposed on the SE lobe spectra for earlier epochs with a dotted line. A linear display scale is used, and constant offsets are applied to the normalized spectra as noted at the left in each panel.

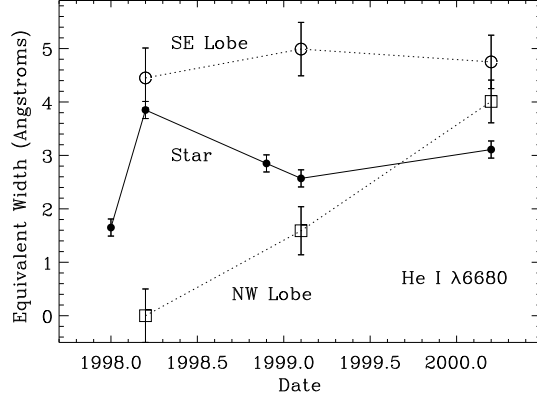


Fig. 14.— Equivalent width of the He I $\lambda 6680$ emission line measured at several different epochs for the star, and reflected spectra from the NW and SE polar lobes (see Figure 13).

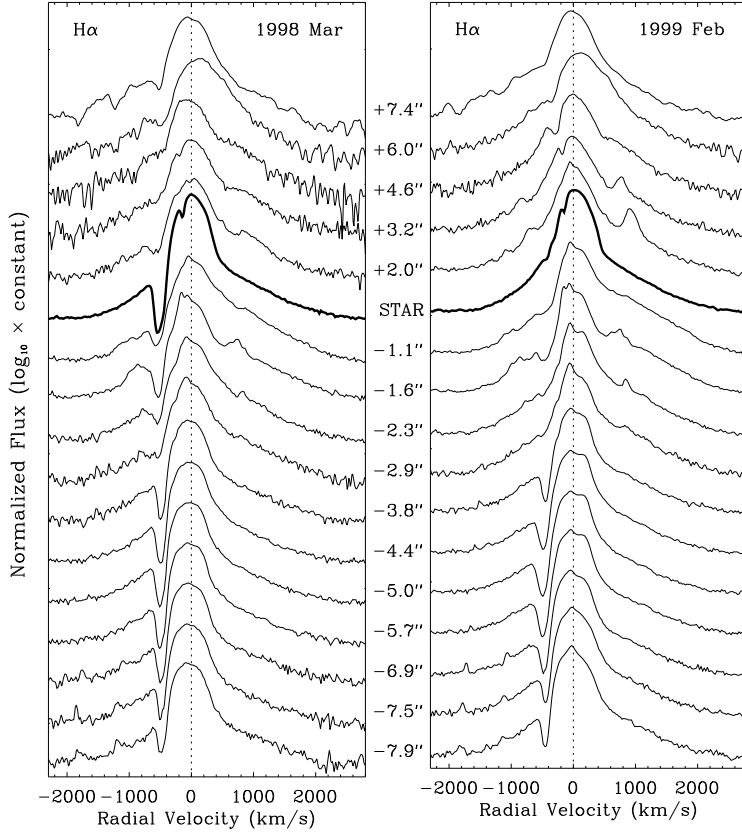


Fig. 15.— Same as Figure 4 but for H α at two different times, March 1998 (left) and February 1999 (right). These tracings correspond to the grayscale H α long-slit spectra in Figure 12, with the slit P.A. oriented at 332° and offset $0.^{\prime}4$ NE of the star. Offset positions are the same for both dates and all are indicated between the two panels.

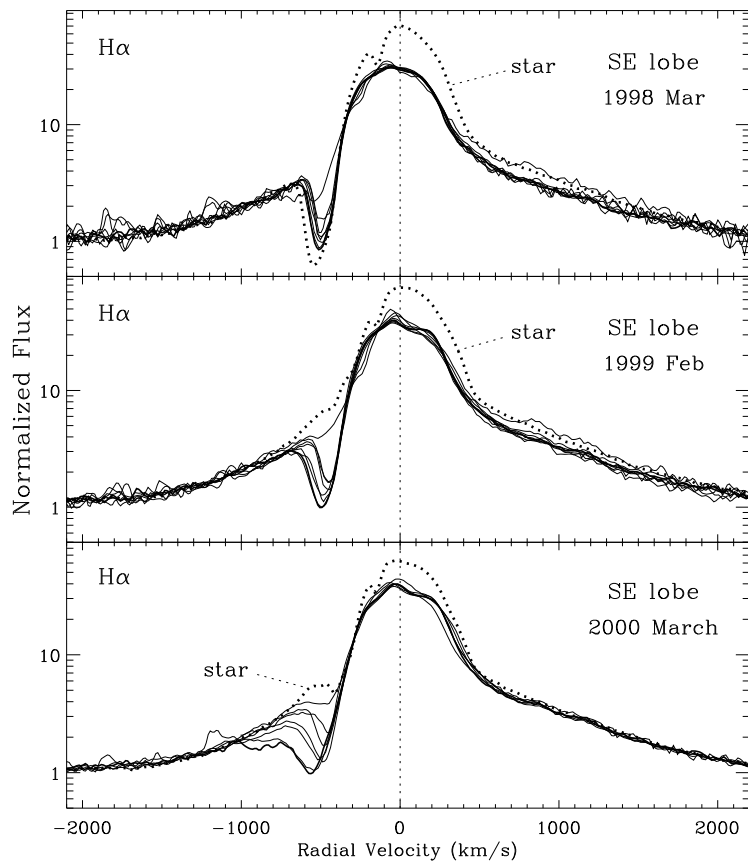


Fig. 16.— Similar to Figure 5 but for H α at three different times, March 1998, February 1999, and March 2000. These tracings in 1998 and 1999 correspond to the grayscale H α long-slit spectra in Figure 13, with the slit P.A. oriented at 332° and offset 0''.4 NE of the star. March 2000 tracings are the same as in Figure 5. The H α profile of the central star is shown by the dotted line for each date.

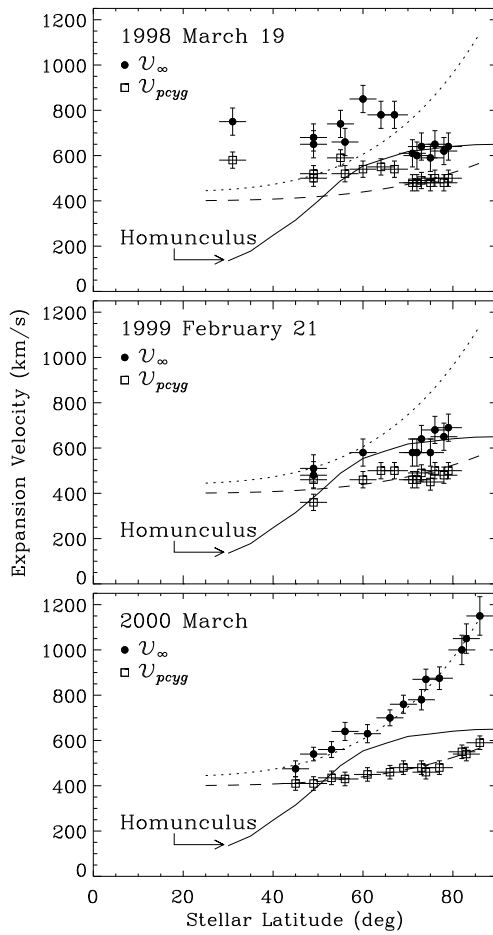


Fig. 17.— Variation of v_{∞} and v_{pcyg} for the H α line as a function of stellar latitude in η Car's stellar wind. Same as Figure 7, but for all three epochs, including March 1998 and February 1999 (see Table 2), and March 2000 (Table 1).

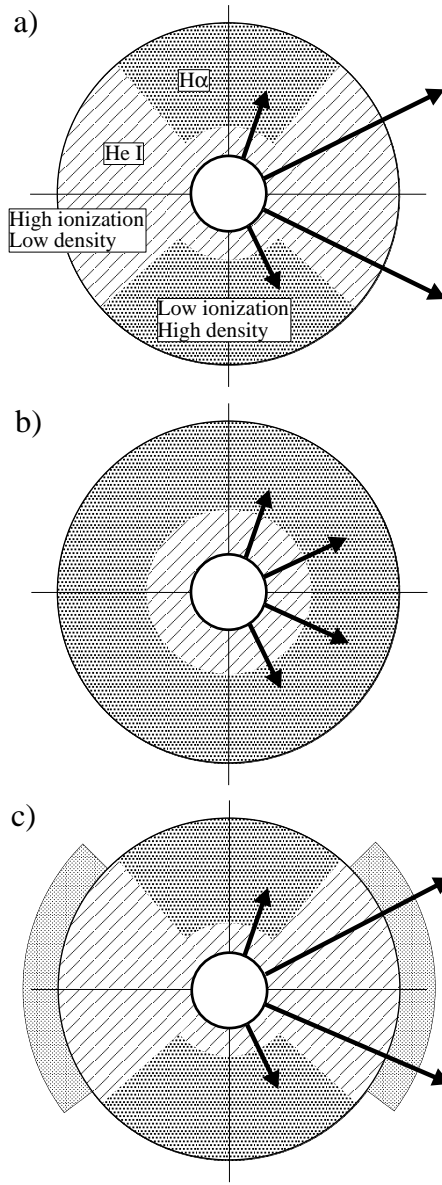


Fig. 18.— Cartoon representing the structure of η Car's wind before (a), during (b), and after (c) a spectroscopic event as indicated by changes in reflected emission line profiles in STIS spectra. Thick black arrows represent hard UV radiation. See also Figure 12. The extra shaded regions to either side in panel (c) represent a thinning shell ejected during the event. This is not intended to be a scale drawing in radius, and the real boundaries between latitudinal zones are not so sharp.